Journal Pre-proof

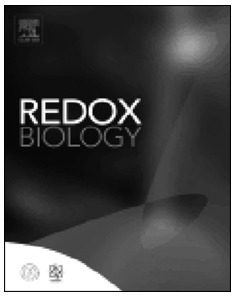

Regulation of metastasis suppressor NME1 by a key metabolic cofactor coenzyme A

Bess Yi Kun Yu, Maria-Armineh Tossounian, Stefan Denchev Hristov, Ryan Lawrence, Pallavi Arora, Yugo Tsuchiya, Sew Yeu Peak-Chew, Valeriy Filonenko, Sally Oxenford, Richard Angell, Jerome Gouge, Mark Skehel, Ivan Gout

PII: S2213-2317(21)00126-9

DOI: https://doi.org/10.1016/j.redox.2021.101978

Reference: REDOX 101978

To appear in: *Redox Biology*

Received Date: 7 February 2021

Revised Date: 28 March 2021

Accepted Date: 13 April 2021

Please cite this article as: B.Y.K. Yu, M.-A. Tossounian, S.D. Hristov, R. Lawrence, P. Arora, Y. Tsuchiya, S.Y. Peak-Chew, V. Filonenko, S. Oxenford, R. Angell, J. Gouge, M. Skehel, I. Gout, Regulation of metastasis suppressor NME1 by a key metabolic cofactor coenzyme A, *Redox Biology*, https://doi.org/10.1016/j.redox.2021.101978.

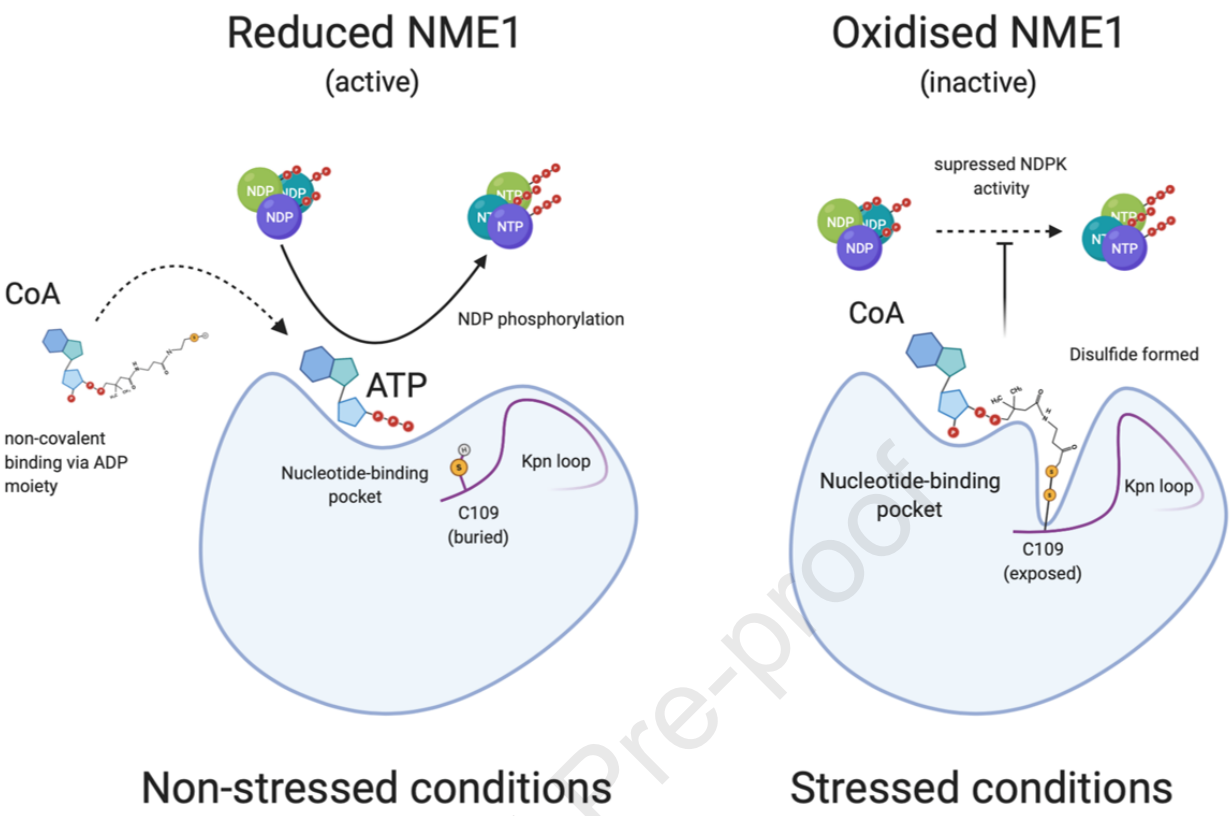

Regulation of metastasis suppressor NME1 by a key metabolic cofactor coenzyme A

Bess Yi Kun Yu[a#], Maria-Armineh Tossounian[a#], Stefan Denchev Hristov[a], Ryan Lawrence[a], Pallavi Arora[a], Yugo Tsuchiya[a], Sew Yeu Peak-Chew[b], Valeriy Filonenko[c], Sally Oxenford[d], Richard Angell[d], Jerome Gouge[e], Mark Skehel[b], and Ivan Gout[a,c*]

[a]Department of Structural and Molecular Biology, University College London, London WC1E 6BT, United Kingdom.
[b]MRC Laboratory of Molecular Biology, Cambridge Biomedical Campus, Cambridge CB2 0QH, United Kingdom.
[c]Department of Cell Signaling, Institute of Molecular Biology and Genetics, Kyiv 143, Ukraine.
[d]School of Pharmacy, University College London, London WC1N 1AX, United Kingdom.
[e]Institute of Structural and Molecular Biology, Birkbeck College, London WC1E 7HX, United Kingdom.

[#]These authors contributed equally to this study
*Co-corresponding author: i.gout@ucl.ac.uk

Declaration of interest: none

Abbreviations

NDPK – Nucleoside diphosphate kinase; NME – non-metastatic protein; CoA – Coenzyme A, CoASSCoA – CoA disulfide; ATP – adenosine triphosphate, ADP – adenosine diphosphate; PTM – post-translational modifications; LC-MS/MS – liquid chromatography tandem mass spectrometry

Abstract

The metastasis suppressor protein NME1 is an evolutionarily conserved and multifunctional enzyme that plays an important role in suppressing the invasion and metastasis of tumour cells. The nucleoside diphosphate kinase (NDPK) activity of NME1 is well recognized in balancing the intracellular pools of nucleotide diphosphates and triphosphates to regulate cytoskeletal rearrangement and cell motility, endocytosis, intracellular trafficking, and metastasis. In addition, NME1 was found to function as a protein-histidine kinase, 3'-5' exonuclease and geranyl/farnesyl pyrophosphate kinase. These diverse cellular functions are regulated at the level of expression, post-translational modifications, and regulatory interactions. The NDPK activity of NME1 has been shown to be inhibited *in vitro* and *in vivo* under oxidative stress, and the inhibitory effect mediated via redox-sensitive cysteine residues. In this study, affinity purification followed by mass spectrometric analysis revealed NME1 to be a major coenzyme A (CoA) binding protein in cultured cells and rat tissues. NME1 is also found covalently modified by CoA (CoAlation) at Cys109 in the CoAlome analysis of HEK293/Pank1β cells treated with the disulfide-stress inducer, diamide. Further analysis showed that recombinant NME1 is efficiently CoAlated *in vitro* and in cellular response to oxidising agents and metabolic stress. *In vitro* CoAlation of recombinant wild type NME1, but not the C109A mutant, results in the inhibition of its NDPK activity. Moreover, CoA also functions as a competitive inhibitor of the NME1 NDPK activity by binding non-covalently to the nucleotide binding site. Taken together, our data reveal metastasis suppressor protein NME1 as a novel binding partner of the key metabolic regulator CoA, which inhibits its nucleoside diphosphate kinase activity via non-covalent and covalent interactions.

Keywords: NDPK, coenzyme A, protein CoAlation, oxidative stress, metastasis suppressor, redox regulation

1. Introduction

Nucleoside diphosphate kinases (NDPKs) are multifunctional enzymes found in organisms across all domains of life (1). The NDPKs are encoded by the non-metastatic, *NME* gene family in humans. Currently, there are 10 known members of the NME family, which form two groups based on sequence homology and conservation of NDPK functionality (1). The members of group I (NME1-4) share 40-88% sequence homology and possess NDPK activity. Members belonging to group II (NME5-10) share only between 6-22% sequence homology and exhibit little to no NDPK activity (1, 2).

NME1 is the most widely studied member of this family, mainly because of its metastasis suppressor function (3). NME1 mainly functions to control intracellular nucleotide homeostasis by catalysing the transfer of a phosphate group from nucleoside triphosphates (NTPs), mainly ATP, to nucleoside diphosphates (NDPs) by a ping-pong mechanism involving the formation of a phosphohistidine intermediate (1). This histidine residue, along with the Kpn-loop and conserved nucleotide-binding pocket are defining features of functional NDPK enzymes. In addition to the NDPK activity, NME1 was found to function as a protein-histidine kinase, 3'-5' exonuclease and geranyl/farnesyl pyrophosphate kinase. Therefore, it is regarded as a moonlighting enzyme (2, 4).

Structure-function studies of native human NME1 revealed a homo-hexameric structure stabilized by cross-interaction between the Kpn-loop region and the neighbouring C-terminal domain. Furthermore, oligomerisation of NME1 into a hexameric structure is required for its phosphotransferase activity either towards NDP phosphorylation or protein-histidine phosphorylation, and the suppression of tumour metastasis (5). The structure and function of NME1 have been shown to be modulated by reactive oxygen species (ROS) via three redox-sensitive cysteine residues. Under oxidative stress, an intramolecular disulfide bridge between Cys4 and Cys145 is formed and triggers an overall conformational rearrangement that destabilizes the hexameric state, resulting in the formation of dimers (6, 7). This conformational change influences the Kpn-loop region which is essential for hexamerization and NDPK activity. Furthermore, NME1 was found to be glutathionylated at Cys109 in cells and *in vitro*, and this modification inhibits its NDPK activity (7). The C109A mutant is resilient to oxidative stress, shows constitutively active NDPK activity and suppresses metastatic growth *in vivo* (6, 7). These findings suggest that the function of NME1 is redox regulated and may be implicated in redox signalling.

The expression, subcellular localisation and function of NME1 are regulated at various levels, including transcription, translation, post-translational modifications and

regulatory interactions. Upregulation of *NME1* gene expression was found in cells upon ligand-induced activation of glucocorticoid receptor and oestrogen receptor α (8, 9). Epigenetic downregulation by means of DNA methylation of CpG islands in the promoter region of NME1 has also been reported (10). The cellular level of NME1 protein is regulated via a ubiquitin-dependent proteasomal degradation pathway mediated by the E3 Ub Ligase FBXO24, or by sequestration to the lysosome (11, 12). A number of NME1 binding partners have been identified, including NME2 and NME4, small GTPase CDC42, kinase suppressor of Ras, large GTPases dynamin 1/2, the GDP-GTP exchange factor TIAM1, DNA repair and redox regulation transcriptional factor APAX1, and pro-apoptotic protease granzyme A (3). NME1 depends on a diverse range of binding partners and regulators to fulfil its roles in regulating not only intracellular nucleotide homeostasis, but also endocytosis, intracellular trafficking, cell motility and metastasis (1).

NME1 was the first metastasis suppressor gene to be identified and subsequent studies revealed around 30 members of this family (13). In contrast to tumour suppressor genes, metastasis dissemination regulators inhibit metastatic dissemination, but not the growth of the primary tumour. The anti-metastatic activity of NME1 has been demonstrated in cell-based and animal models by various laboratories. These studies revealed that: a) stable overexpression of NME1 in highly metastatic cell lines results in significant reduction of their metastatic potential in xenograft models (14, 15); b) the increase in lung metastases is observed in NME1 deficient mice prone to develop hepatocellular carcinoma (16); and c) siRNA-mediated knockdown of *NME1* promotes metastatic potential in non-invasive cancer cell lines (17).

Coenzyme A (CoA) is a low molecular weight thiol, which is produced in all living cells by an enzymatic conjugation of ATP, pantetheine and cysteine (18, 19). The presence of a highly reactive thiol group allows CoA to bind short-, medium- and long-chain carboxylic acids which are transported into cells or produced during catabolic and anabolic processes. A diverse range of metabolically active CoA thioesters (acetyl-CoA, malonyl-CoA, HMG-CoA among others) are produced in cells to drive cellular metabolism, signal transduction and gene expression. The levels of CoA and its thioester derivatives are tightly controlled by various extracellular and intracellular stimuli, including hormones, nutrients, metabolites and oxidative stress (20-23). The pathogenesis of various human diseases has been associated with dysregulated CoA biosynthesis and homeostasis, including cardiac hypertrophy, metabolic disorders and cancer (24-27). Inborn mutations in the human genes of the CoA biosynthetic pathway have been implicated in the development of neurodegeneration (pantothenate kinase 2 and CoA synthase) and dilated cardiomyopathy (phosphopantothenoylcysteine synthetase) (28-30).

The antioxidant function of CoA in redox regulation has been recently discovered. CoA was shown to employ its highly reactive thiol group for covalent modification of solvent-exposed cysteine residues in cellular response to oxidative or metabolic stress. This novel post-translational modification (PTM) was termed protein CoAlation and shown to be a widespread and reversible mechanism of redox regulation (31-37). To date, more than 2200 proteins have been found to be CoAlated in prokaryotic and eukaryotic cells with the use of a mass spectrometry-based methodology and highly specific anti-CoA monoclonal antibody (35, 36, 38, 39). Bioinformatic analysis showed that the vast majority of CoAlated proteins are involved in metabolic processes, as well as the antioxidant response and protein synthesis. Recent studies revealed that protein CoAlation regulates the activity, conformation and subcellular localisation of modified protein, and protects cysteine residues from irreversible overoxidation (31-37, 40).

In this study, we demonstrate for the first time that all four members of the Group I NME family of proteins specifically associate with CoA affinity matrices during the purification of CoA binding partners from mammalian cell and tissue lysates. Furthermore, NME1 was found to be among CoAlated proteins in mammalian cells treated with the disulfide-stress inducer, diamide. Therefore, our efforts have been focused on investigating NME1 CoAlation *in vitro* and *in vivo*, and the regulation of its NDPK activity by CoA binding. We showed that recombinant NME1 is efficiently CoAlated *in vitro*, and oxidising agents and metabolic stress induce covalent modification of NME1 by CoA in cells. Furthermore, the NDPK activity of *in vitro* CoAlated NME1 is inhibited and the inhibition is reversed by the reducing agent DTT. We also found that CoA can function as a competitive ATP-binding inhibitor of the NME1 NDPK activity. Altogether, these findings uncover a novel mode of NME1 regulation by a key metabolic integrator CoA, which is particularly pronounced in cellular response to oxidative or metabolic stress.

2. Materials and Methods

2.1. Reagents and Chemicals

Unless otherwise stated, all common reagents and chemicals were obtained from Sigma-Aldrich, including ATP, CoA monomer, CoA disulfide (CoASSCoA), hydrogen peroxide (H_2O_2), 2′-deoxycytidine 5′-diphosphate sodium salt (dCDP), phosphoenolpyruvate (PEP) pyruvate kinase (PK), lactate dehydrogenase (LDH), N-ethylmaleimide (NEM), diamide, and coenzyme A (CoA)-agarose. The generation and characterisation of the mouse anti-CoA monoclonal antibody 1F10 has been previously described (38). Other antibodies used were rabbit anti-NME1 polyclonal antibody (WB dilution 1:2000, Proteintech® Europe); Alexa

Fluor 680 goat anti-mouse IgG H&L (WB dilution 1:10 000, Life Technologies) and IRdye 800 CW goat anti-rabbit IgG H&L (WB dilution 1:10 000, LI-COR Biosciences).

2.2. Plasmids and mutagenesis

pTwistCMV-Hygro and pET28a(+) plasmids containing a C-terminal Flag-tagged or an N-terminal 6xHis-tagged human NME1 cDNA (CR542104.1), respectively, were synthesised by TwistBiosciences. *h*NME1 cDNA sequence within the pET28a(+)-His-*h*NME1 plasmid was codon optimized for protein expression in *Escherichia coli* BLR (DE3) cells.

To substitute the Flag-tag with a 6xHis-tag within the pTwistCMV-Flag-*h*NME1 plasmid, the plasmid was amplified using phosphorylated primers, one of which contained an overhang with the His-tag sequence. After amplification, the PCR product was circularized using T4 DNA ligase (Thermo Scientific), and transformed in *E. coli* Top10 cells. The phosphorylated primers used were; Forward primer 5'-P-CATCATCATCATCATCATTGAGGATCCGCAG GCCTCT-3') and reverse primer 5'-P-GCTGCCTTCATAGATCCAGTTCTGAGC-3'). The final sequence of His-*h*NME1 in pTwistCMV-*h*NME1-His plasmid was confirmed by Sanger sequencing.

To mutate the *h*NME1 Cys109 residue to an Ala109, site-directed mutagenesis was performed as described in the QuickChangeXL site-directed mutagenesis protocol (Agilent Technologies). A single point mutation was introduced in the pET28a(+)-His-*h*NME1 plasmid. Forward primer 5'-GGTACGATTCGCGGGGATTTCGCTATTCAGGTAGGACGC AATATC-3' and reverse primer 5'-GATATTGCGTCCTACCTGAATAGCGAAATCCCCGC GAATCGTACC-3' were used to generate the pET28a(+)-His-*h*NME1 C109A mutant plasmid.

2.3. Generation of CoA affinity matrices and affinity purification of CoA-binding proteins

The CoA-sulfolink matrix was generated by coupling the SulfoLink® Coupling Resin (Thermo Scientific) to coenzyme A (5 mg CoA/500 µL bead-volume) in coupling buffer (50 mM Tris-HCl pH 8.5, 5 mM ethylenediaminetetraacetic acid (EDTA)) by end to end mixing at room temperature (RT) for 2 h. Non-specific binding sites on the beads were then blocked with 50 mM L-Cysteine-HCl and 25 mM tris(2-carboxyethyl)phosphine (TCEP) for 45 min at RT. The CoA-bound resins were washed 4 times with 8X bead-volume with 1 M NaCl. Finally, the generated CoA-sulfolink beads were washed with 6X bead-volume of 50 mM Tris-HCl pH 7.5, 150 mM NaCl, 2 mM EDTA, supplemented with 0.02% sodium azide for storage at 4˚C in a 50% suspension. All washes were done by centrifugation at 4˚C at 956 x*g* for 2 min.

The CoA-agarose and Tris-agarose matrices were regenerated from lyophilised beads (Sigma-Aldrich) in 10X bead volume of expansion buffer (50 mM Tris-HCl pH 7.5, 150 mM

NaCl, 2 mM EDTA). Matrices were washed three times with bead-volume of expansion buffer and stored in a 50% suspension with supplementation of 0.02% sodium azide.

2.4. Preparation of rat tissue and cell lysates, and affinity purification of CoA-binding proteins

All experiments involving animals were performed in accordance with the European Convention for the Protection of Vertebrate Animals used for Experimental and Other Scientific Purposes (CETS no.123) and the UK Animals (Scientific Procedures) Act 1986 amendment regulations 2012.

Rat liver, kidney, brain and heart were harvested from pentobarbitone-anaesthetised rats (300 mg/kg of body weight) and immediately freeze-clamped using tongs pre-cooled in liquid nitrogen (N_2). Using a tissue tearor, frozen organs were powdered in liquid N_2 and homogenised in ice-cold lysis buffer, which is composed of 50 mM Tris-HCl pH 7.5, 150 mM NaCl, 5 mM EDTA, 50 mM NaF, 5 mM $Na_2P_4O_7$, and 1% triton X-100, supplemented with 100 mM NEM and 1X cOmplete Mini protease inhibitor cocktail (PIC, Roche). Tissue lysates were centrifuged at 53,000 xg (Beckman JA-25.50 rotor) for 5 min at 4˚C. The supernatant was used for affinity purification of CoA-binding proteins.

~2 million HEK293/Pank1β cells were seeded onto 100 mm plates. To induce diamide stress, cells were treated at 37˚C with 500 µM diamide for 30 min or treated and left to recover in full Dulbecco's Modified Eagle Medium (DMEM) for another 30 min. Cells were harvested by pressure washing and centrifuged at 1,800 xg for 5 min at RT. Cells were lysed with 500 µL of lysis buffer supplemented with 100 mM NEM and 1X PIC, and incubated on ice for 20 min before centrifugation at maximum speed for 15 min at 4˚C. The supernatant was used for affinity purification of CoA-binding proteins.

To pull-down CoA-binding proteins from rat tissues and HEK293/Pank1β cells, prepared lysates were divided into 3 equal parts and first incubated with 20 µL Tris-agarose (50% suspension) for 18 h at 4˚C by end to end mixing. The supernatant was collected and further incubated with 20 µL Tris-agarose, or CoA-agarose or CoA-sulfolink matrices for 3 h at 4˚C. After incubation, beads were washed three times with lysis buffer (50 mM Tris-HCl pH 7.5, 150 mM NaCl, 5 mM EDTA, 50 mM NaF, 5 mM $Na_2P_4O_7$, and 1% triton X-100) by centrifugation (956 xg, 2 min, 4˚C). Bound proteins were released from beads through boiling in sodium-dodecyl-sulphate (SDS) loading buffer (1x) for 5 min and analysed by SDS-PAGE under reducing conditions.

2.5. Mammalian cell culture, transfection and treatment with oxidising agents and metabolic stress

HEK293/Pank1β cells stably overexpressing pantothenate kinase 1β (HEK293/Pank1β) were generated as previously described (35). HEK293/Pank1β cells were maintained in

DMEM supplemented with 10% foetal bovine serum (FBS, Gibco), 50 U/mL penicillin and 0.25 μg/mL streptomycin (Lonza). Cells were cultured at 37˚C and 5% CO_2.

Approximately 0.6 million HEK293/Pank1β cells were seeded onto 60 mm plates and transiently transfected at ~60% confluency with TwistCMV-6xHis-*h*NME1 plasmid using TurboFect reagent (Thermo Scientific), according to the manufacturer's protocol. Transfected cells were grown for 24 h in complete DMEM with 10% FBS. To prime cells for oxidative stress, the medium was replaced with glucose- and pyruvate-free DMEM supplemented with 5 mM glucose and 10% FBS and cells were incubated for another 24 h. Cells were then treated at 37˚C with diamide (500 μM – 30 min) or H_2O_2 (100 μM, 500 μM, 1 mM, 2.5 mM – 30 min). To induce metabolic stress, the media of cells were changed to glucose- and pyruvate-free DMEM for 20 h. Cells were harvested by pressure washing and centrifuged at 1,800 xg for 5 min at room temperature (RT). Cells were lysed with 300 μL of lysis buffer supplemented with 100 mM NEM and 1X PIC, and incubated on ice for 20 min before centrifugation at maximum speed for 15 min at 4˚C. The supernatant was used for SDS-PAGE or affinity purification analysis.

2.6. Exposure of bacterial cells to oxidising agents or nutrient deprivation

Escherichia coli BL21 (DE3) cells were transformed with the pET28a(+)-His-*h*NME1 plasmid. Cells were cultured in LB medium at 37°C to mid-log phase (OD_{600} = 0.7) and the expression of His-*h*NME1 was induced with 0.5 mM isopropyl β-D-1-thiogalactopyranoside (IPTG) for 3 h at 25°C. Oxidative stress was then induced by culturing bacteria for 10 min at 37°C with 2 mM diamide, or 10 mM H_2O_2. To induce hypochlorite (NaOCl) stress, the IPTG-induced bacterial culture was pelleted, resuspended in warm M9 minimal media (M9), and incubated for 5 min at 37°C, before the 10 min-treatment with 100 μM NaOCl. Cells were lysed with bacterial lysis buffer (50 mM Tris-HCl pH 7.5, 50 mM NaCl, 5 mM EDTA) supplemented with 25 mM NEM, 0.1 mg/ml lysozyme and 1X PIC. The lysates were incubated on ice for 20 min and mixed with an equal volume of 2% SDS, sonicated on ice in the Soniprep 150 over 5 cycles of 5 s pulse ON and 20 s pulse OFF to reduce viscosity and centrifuged at 21 000 xg for 20 min at 4°C. The supernatant was mixed with non-reducing loading buffer and heated at 95°C for 5 min. His-*h*NME1 was pulled-down from the supernatant using Talon affinity matrix (Generon) and analysed together with total cell lysates by SDS–PAGE under non-reducing condition and Western blotting with anti-CoA antibody.

2.7. Expression and Purification of 6XHis-hNME1 wild type (WT) and C109A mutant

A single colony of *Escherichia coli* BLR (DE3) cells containing pET28a(+)-His-*h*NME1 or pET28a(+)His-*h*NME1 C109A mutant plasmid was grown overnight in Luria Broth (LB, Miller) supplemented with 25 μg/mL kanamycin. The preculture was diluted 1:100 in 1 L LB medium

and grown at 37°C until an OD_{600} of 0.7 was reached. After induction with 0.5 mM IPTG, the cells were grown for 18 h at 25°C. The cells were harvested by centrifugation (15 min at 6,200 xg, at 4˚C; Beckman JLA 8.1000 rotor). The pellet was resuspended in 50 mM Tris-HCl pH 7.5, 500 mM NaCl, 1 mM β-mercaptoethanol, 50 μg/mL DNase I and 10 mM $MgCl_2$, supplemented with 1X PIC and sonicated on ice in the Soniprep 150 over 15 cycles of 15 s pulse ON and 30 s pulse OFF at 4˚C. Following sonication, the samples were centrifuged at 39,000 xg at 4°C for 30 min (Beckman JA-25.50 rotor). The cell lysate was loaded onto a Xk16/20 column (GE Healthcare) packed with TALON affinity resin (Generon), equilibrated in 50 mM Tris-HCl pH 7.5, 500 mM NaCl, 1 mM β-mercaptoethanol, and 10 mM $MgCl_2$. With an ÄKTA™start system (GE Healthcare), the protein was eluted using a linear gradient to 0.25 M imidazole in the same buffer. His-*h*NME1 WT and C109A were dialyzed to 50 mM Tris-HCl pH 7.5, 500 mM NaCl, 10 mM $MgCl_2$ and 2 mM dithiothreitol (DTT). Proteins were stored in 10% glycerol at -20°C until use.

2.8. In vitro CoAlation of His-hNME1 WT and C109A mutant

Purified recombinant His-*h*NME1 WT and C109A mutant were reduced with 20 mM DTT for 30 min at 25˚C. Micro Bio-Spin™6 columns (Bio-Rad) were used to remove excess DTT. NME1 CoAlation assay was performed in nitrogen (N_2)-flushed assay buffer composed of 20 mM Tris-HCl pH 8.0, and 100 mM NaCl. Reduced His-*h*NME1 WT or C109A (100 μM) was incubated with CoA (400 μM) in the presence and absence of CoA dimer (CoASSCoA, 400 μM) for 1.5 h at 25˚C. For oxidising conditions, recombinant proteins were incubated with CoA (700 μM) for 5 min and a further 1 h and 25 min in the presence of H_2O_2 (2 mM). The reactions were stopped by passing the reaction mixture through a Micro Bio-Spin™ 6 column to remove excess CoA, CoASSCoA or H_2O_2. NME1 CoAlation was confirmed by Western blotting with anti-CoA antibodies. Samples were used in further NDPK activity assays. For Western blotting or Coomassie-stain analysis of *in vitro* NME1 CoAlation, samples were incubated with 100 mM NEM for 10 min at 25˚C and boiled in 1x SDS loading buffer in the presence or absence of 100 mM DTT for 5 min at 95˚C.

2.9. Western Blot Analysis

The concentration of protein lysates from rat tissue lysates and HEK293/Pank1β were measured using the Bicinchoninic acid assay (BCA, Thermo Scientific). Samples were mixed with SDS loading buffer (1X) in the presence or absence of DTT, and boiled for 5 min. 20 μg of protein lysates (rat tissues or HEK293/Pank1β) or 0.5 μg of recombinant NME1 WT and C109A mutant were separated by SDS-PAGE in a 4-20% Precast Gel (Sigma-Aldrich) and subsequently transferred to a low-fluorescence PVDF membrane (Merck, Millipore). Following transfer, the membrane was blocked with Intercept® (TBS) Protein-Free blocking

buffer (LI-COR Biosciences) for 20 min at RT. The PVDF membrane was subsequently incubated with mouse anti-CoA primary antibodies (1:6000) or rabbit anti-NME1 primary antibodies (1:3000, Proteintech) at 4˚C overnight or 2 h at RT. The membranes were washed extensively with Tris-buffer saline supplemented with 0.05% Tween 20 (TBSt) before incubation with the secondary anti-mouse (1:10 000) and anti-rabbit antibodies (1:10 000) for 30 min at RT. The immunoreactive bands were visualised using Odyssey Scanner CLx and analysed with Image Studio Lite software (LI-COR Biosciences).

2.10. NDPK Activity Assay

The assay was performed as described previously (41, 42). In brief, the NDPK activity assay was carried out in a 200 μL reaction mixture in a BRAND® 96-well plate (Sigma-Aldrich), containing 250 μM NADH (Grade II, purity >98%, Roche), 2.5 U LDH, 2 U PK, 0.2 mM dCDP, 2 mM ATP and 0.3 mM PEP. The reaction was initiated by the addition of 25 nM His-*h*NME1 WT or C109A mutant. The CoAlated samples of NME1 were prepared via incubation with CoA and CoASSCoA as described in section 2.8. and the reaction was stopped by buffer exchange using the Micro Bio-Spin™6 columns. The absorbance values at 340 nm were measured at 10 s intervals over a period of 5 min using the FLUOstar OPTIMA microplate reader. Specific NDPK activity was calculated with the following equation (Equation 1); where the extinction coefficient of NADH is ε= 6220 $M^{-1}cm^{-1}$, l represents the pathlength (0.222 cm), $\Delta Abs340_{Sample}$ represents the change in absorbance at 340 nm of sample, and $\Delta Abs340_{Buffer}$ represents the change in absorbance at 340 nm of buffer.

Equation 1:

$$Specific\ NDPK\ activity\ \left(\frac{U}{mL}\right) = \frac{\left[\left(\Delta Abs340_{Sample} - \Delta Abs340_{Buffer}\right) x\ 60\ s\ \right] x\ 1000}{\varepsilon(M^{-1}cm^{-1})\ \ x\ l\ (cm)}.$$

The NDPK activity was measured from at least three independent replicates. The values of specific NDPK activity were subsequently converted to percentage NDPK activity (%) by comparing to the reduced NME1 WT and NME1 C109A activity. For statistical analysis, a Šidák multiple comparison, ordinary one-way ANOVA test was used assuming unequal variances with GraphPad Prism (Version 9.1.0). The statistical significance established have been indicated in the figure legends with p values defined and the statistical variability was estimated with the standard error of the mean (SEM).

2.11. NDPK Activity Inhibition Assay

The NDPK activity assay of NME1 WT and C109A mutant were performed as described in section 2.10, with the exception of the addition of increasing concentrations of CoA (0, 2, 4

mM) within the reaction mixture. The NDPK activity was measured from at least three independent replicates. The values of specific NDPK activity were subsequently converted to percentage NDPK activity (%) by comparing to the reduced NME1 WT and NME1 C109A activity.

2.12. Mass Spectrometry and Data Processing

2.12.1. Trypsin Digestion and Nudix7 Cleavage

Liquid Chromatography-mass spectrometry (LC-MS/MS) identification of CoAlated peptides from diamide-treated HEK293/Pank1β cells (Supplementary Table 1) and excised gel bands of 17 kDa (Figure 1C & D) was carried out as previously described (35). Excised gel bands were destained with acetonitrile (MeCN), and alkylated with 50 mM iodoacetamide (IAM) in 50 mM ammonium bicarbonate (pH 7.8), in the dark at RT. Gel bands were digested overnight with 7 ng/µL of trypsin (Promega, UK) in 50 mM ammonium bicarbonate, 5 mM IAM, at 37°C. Peptides were extracted initially with 2% formic acid (FA), followed by 30% MeCN/0.5% FA. Prior to LC/MS analysis, the combined peptide mixtures were partially dried down in a Speed Vac (Savant, Fischer Scientific) to remove the MeCN. Proteins from diamide-treated HEK293/Pank1β lysates were precipitated with 90% methanol (-20°C) by vortexing and pelleted by centrifugation at 5,000 xg for 20 min at 4°C. The protein pellet was homogenised for 30 s at RT in 1.5 mL of 90% methanol with a tissue tearor to remove free CoA, CoA esters, LMW thiols, and adenine nucleotides. 50 µL of the homogenate was aliquoted and resolubilised with 100 mM Tris-HCL pH 7.5, 5 mM EDTA, 0.5% SDS, 6 M urea to determine the protein concentration using BCA assay. The remaining homogenate was centrifuged at 18,000 xg for 3 min at RT before partial-drying with a Speed Vac for 6 min. The protein pellet was digested for 90 min at 30°C with enzyme/protein ratio 1:200 of LysC (mass-spec grade, Promega, UK) in 50 mM ammonium bicarbonate supplemented with 6.4 mM IAM and further digested with 7 ng/µL of trypsin at 30°C for 10 h. The trypsinised samples were heat-inactivated, followed by the incubation with anti-CoA monoclonal antibodies, which were cross-linked to Protein G-Sepharose. Immunoprecipitated peptides were eluted from beads with 0.1% trifluoroacetic acid and dried completely in a speed vac concentrator. The resulting pellet was resolubilised in 20 µL of 50 mM ammonium bicarbonate. 2.3 µL of 50 mM $MgCl_2$ and 1 µL of Nudix 7 (1.7 µg) were added and incubated at 37°C for 30 min. The peptide mixtures were acidified and desalted using home-made C18 (3M Empore) stage tip that contained 1.5 µL of poros R3 (Applied Biosystems) resin. Bound peptides were eluted sequentially with 15 µL 30%, 50% and 80% acetonitrile in 0.5% FA, and partially dried down to less than 10 µL. Then, 100 µL of Iron (III)-immobilized metal ion

affinity chromatography (IMAC) binding buffer (30% acetonitrile/ 0.25M acetic acid) was added to the samples, ready for IMAC enrichment.

2.12.2. Iron (III)-immobilized metal ion affinity chromatography (IMAC) enrichment

PhosSelect iron affinity gel (IMAC beads, Sigma Aldrich, cat. P9740) was washed three times with 100 µL of IMAC binding buffer and prepared as 50% slurry. 15 µL were added to the samples and incubated at room temperature for 45 min, with vigorous shaking. The beads were transferred to a home-made C8 (3M Empore, USA) stage tip and washed 4 times with 30 µL binding buffer. Bound peptides were eluted sequentially with 30 µL of 500 mM imidazole pH 7.6, 30% MeCN/500 mM imidazole pH 7.6 and 50% MeCN/ 0.5% FA. The combined eluates were acidified, partially dry down in a Speed Vac and desalted using home-made C18 (3M Empore, USA) stage tip that contained 0.8 µL of poros R3 (Applied Biosystems, UK) resin. Bound peptides were eluted sequentially with 30%, 50% and 80% acetonitrile in 0.5% FA, and partially dried down, ready for MS analysis.

2.12.3. LC-MS/MS analysis

Peptide mixtures were separated by nano-scale capillary LC-MS/MS using an Ultimate U3000 HPLC (ThermoScientific Dionex, San Jose, USA) to deliver a flow of approximately 300 nL/min. A C18 Acclaim PepMap100 5 µm, 100 µm x 20 mm nanoViper (ThermoScientific Dionex, San Jose, USA), trapped the peptides prior to separation on a C18 Acclaim PepMap100 3 µm, 75 µm x 250 mm nanoViper (ThermoScientific Dionex, San Jose, USA). The column was developed with an acetonitrile gradient, consisting of buffer A (2% MeCN, 0.1% formic acid) and buffer B (80% MeCN, 0.1% formic acid). Peptides from solution digests were eluted using a gradient of 3 to 10 % B in 49 min, 10-35% in 70 min and 35-90% in 7 min, while gel bands digest were eluted with a gradient of 6-45% B in 31 min and 45-90% B in 15 min. The analytical column outlet was directly interfaced via a nano-flow electrospray ionisation source, with a hybrid quadrupole orbitrap mass spectrometer either a Velos (solution digest) or Q Exactive Plus (gel bands digest) (ThermoScientific, San Jose, USA). The Velos mass spectrometer was operated in standard data dependent mode, performing survey full-scans (m/z 3500-1600) with a resolution of 60,000 at m/z = 400, followed by MS2 acquisitions of the 20 most intense ions in the LTQ ion trap. The Q Exactive plus mass spectrometer was also operated in data dependent mode, performing MS1 full scans (m/z = 380-1600) with a resolution of 70,000, followed by MS2 acquisitions of the 15 most intense ions with a resolution of 17,500.

2.12.4. MaxQuant (MQ) identification of CoAlated peptides

For solution digested samples, the acquired MS/MS raw files were processed using MaxQuant (43) with the integrated Andromeda search engine (v.1.5.2.8) as standard LC/MS identification. MS/MS spectra were searched against a Human UniProt Fasta database. Carbamidomethylation, N-ethylmaleimide, CoA_765, CoA_356 and CoA_338 of cysteines, and oxidation of methionine were set as variable modifications. Enzyme specificity was set to trypsin, with a maximum of two missed cleavages allowed. CoAlated peptides identified were filtered using default settings of a minimum score of 40 for accepting an MS/MS identification for modified peptides. The Andromeda score (Scores, Supplementary Table 1) is calculated as ~10 times the logarithm of the probability of matching at least k out of the n theoretical masses by chance, where k = number of matching ions in a spectrum and n = total number of theoretical ions. The default score of a minimum of >40 was applied, hence, scores higher than 40 are considered confident assignments.

For gel bands, the acquired raw data files were searched using Mascot (Matrix Science, v2.4) against a Human and Rat UniProt Fasta database. Up to two missed cleavages were allowed for a trypsin digest search. Variable modifications were set as carbamidomethylation of cysteines, N-terminal protein acetylation and oxidation of methionine. Scaffold (version 4.8.4, Proteome Software Inc.) was used to validate MS/MS-based peptide and protein identifications. The Normalised Total Spectral Count in Table 1 is determined in Scaffold by a) finding the total number of spectra in each BioSample. b) The average number of spectra across all BioSamples is calculated. c) Scaffold then multiplies each spectrum count by the average over the total for each BioSample.

3. Results

3.1. Affinity purification and mass spectrometric analysis of CoA-binding proteins

The presence of an ADP moiety and a pantetheine tail with a highly reactive thiol group allows CoA to be involved in diverse biochemical reactions and regulatory interactions. Many CoA-binding proteins have been identified and the mode of interaction has been investigated using biochemical, biophysical, and crystallographic approaches (44). The identified interactions were found to occur via non-covalent and dynamic covalent bonds (33, 44). In this study, we searched for novel CoA-binding proteins in rat tissues and cultured cells using two affinity matrices, which have CoA immobilised either via the thiol group (CoA-sulfolink) or the amino group of the ADP moiety (CoA-agarose) (Figure 1A). The orientation of CoA immobilisation to the agarose beads provides a strategy for the affinity purification of proteins that can recognise either a free 3',5'-ADP moiety or a pantetheine tail with a free

thiol (-SH) group, respectively. To eliminate proteins which bind non-specifically to the matrix, Tris-agarose beads were used as a control (Figure 1A).

Initially, all three matrices were incubated with lysates from rat tissues (heart, brain, liver and kidney). After extensive washes, bound proteins have been denatured and separated by SDS-PAGE under reducing conditions. The analysis of the Coomassie-stained gel revealed distinctive patterns of proteins bound to respective matrices. A number of proteins were associated with CoA-agarose and/or CoA-sulfolink matrices, but not with Tris-agarose (Figure 1B). A protein of approximately 17 kDa was notably detectable in CoA-agarose samples from all analysed rat tissues, when compared to control Tris-agarose beads. A protein with a similar molecular weight was also bound to the CoA-sulfolink affinity matrix, but with lower efficacy.

To validate and further extend these findings, we used HEK293 cells with stable overexpression of pantothenate kinase 1β (HEK293/Pank1β). This cell line was shown to produce approximately six times more CoA than parental HEK293 cells, which is comparable to the level of CoA found in rat tissues (heart, liver and kidney) and primary cardiomyocytes (35). To examine the effect of oxidative stress on the pattern of CoA-binding proteins, affinity matrices were incubated with the lysates of exponentially growing HEK293/Pank1β cells (control), cells treated with 500 μM diamide for 30 min (diamide-stressed) or cells recovered from the diamide-induced stress in fresh DMEM media for 30 min (stress-recovered). The analysis of Coomassie-stained gel suggests an enrichment of proteins from HEK293/Pank1β cells bound to CoA-agarose matrix, compared to CoA-sulfolink or Tris-agarose matrices (Figure 1C). Reduced binding to CoA-agarose matrix is detected in diamide-stressed cells, when compared to exponentially growing cells, but this observation requires further validation. Similar to the rat tissue lysates, a band of approximately 17 kDa from HEK293/Pank1β cell lysates was readily detected in both CoA affinity matrices but absent from the control Tris-agarose matrix. In contrast, the observed 17 kDa protein binds with a similar efficacy to both CoA-agarose and CoA-sulfolink affinity matrices in HEK293/Pank1β cell lysates (Figure 1C).

To identify this abundant CoA-binding protein, gel slices of Coomassie-stained bands, corresponding to the 17 kDa protein from rat heart tissue and stress-recovered HEK293/Pank1β cells were processed for mass spectrometric analysis. The LC-MS/MS analysis of tryptic peptides from the rat heart tissue and HEK293/Pank1β cells identified NME1 (NDPKA) and NME2 (NDPKB) as the two most abundant proteins present based on the normalised total spectral count (45), (>95% confidence level) (Table 1). In addition, the other two isoforms of Group I NMEs: NME3 (NDPKC) and NME4 (NDPKD), were also

identified albeit with a lower abundance. These findings suggest that all four members of the Group I NME family (NME1-4) are CoA-binding proteins and that their interaction with CoA is possibly mediated via their nucleotide binding pocket. The normalised total spectrum count which represents protein abundance for all 4 NME isoforms is shown in Table 1. The multiple sequence alignment of NME1-4 is shown in Supplementary Figure 1.

3.2. NME1 is CoAlated at Cys109 in cellular response to oxidative stress

Recent studies from our laboratory demonstrated widespread protein CoAlation in mammalian cells and tissues exposed to oxidative or metabolic stress (36). Using an optimised MS-based methodology, numerous CoAlated proteins have been identified from H_2O_2-perfused rat heart, liver mitochondria of 24 h-starved rats and H_2O_2-treated HEK293/Pank1β cells (36). The extensive protein CoAlation detected in diamide-treated HEK293/Pank1β cells prompted us to determine the identity of CoA-modified proteins (Figure 2A) (36). Diamide-treated HEK293/Pank1β cells were lysed, CoAlated peptides enriched and identified by LC-MS/MS. The MS analysis revealed 498 CoAlated peptides, corresponding to 402 proteins (Supplementary Table 1). Bioinformatic pathway analysis of identified CoAlated proteins showed that they are predominantly involved in metabolic pathways, as well as stress response processes and protein synthesis. In the list of CoAlated proteins, a peptide corresponding to NME1 was found to be CoA-modified (Supplementary Table 1). Figure 2B shows the LC-MS/MS spectrum of a peptide derived from NME1 (GDFCIQVGR) with an increase in 356 Da at cysteine 109 (Cys109), which corresponds to the covalent attachment of 4-phosphopantetheine (a product of CoA cleavage by Nudix7 hydrolase). Cys109 is located in the Kpn-loop of NME1 and is in close vicinity to the active site (Figure 2C). Through cooperative interactions with the C-terminal region of NMEs, the Kpn-loop is important in maintaining the oligomeric stability of the enzymatically active hexamer, and hence is crucial for NDPK activity (46). NME1 is known to be the target for different oxidative post-translational modifications at Cys109, including sulfenylation, sulfonylation, intermolecular disulfide bonding and glutathionylation (7). Therefore, Cys109 was proposed to function as a redox-sensitive switch in regulating the function of NME1 under oxidative stress (7). Interestingly, Cys109 is conserved in NME1-3, but not in the mitochondrially localised NME4 (Figures 2D and S1).

3.3. NME1 is CoAlated in vitro and in bacterial cells exposed to oxidative stress and nutrient deprivation

To validate and further investigate the mode of CoA binding to NME1, we examined CoAlation of recombinant *h*NME1 *in vitro* and in cells exposed to oxidative or metabolic stress. Initially, our efforts were focused on testing covalent modification of NME1 by CoA

using an *in vitro* CoAlation assay. To do so, recombinant *h*NME1 was *in vitro* CoAlated in the presence of CoA and CoA disulfide (CoASSCoA) or CoA and H_2O_2 for 1.5 h at 25˚C. The reaction was stopped by the addition of 10 mM NEM. The samples were separated by SDS-PAGE gel and either analysed by Western blotting with anti-CoA and anti-NME1 antibodies or Coomassie staining (Figure 3A). The Coomassie-stained gel and anti-NME1 Western blot show that recombinant His-*h*NME1 migrates on the SDS-PAGE gel as a ~20 kDa band under reducing and non-reducing conditions (Figure 3A). The anti-CoA Western blot showed that *h*NME1 CoAlation did not occur in the presence of only reduced CoA (control sample - Lane 1), but was induced with the addition CoASSCoA (Lane 2) or H_2O_2 and CoA (Lane 3). Only weak anti-CoA immunoreactive bands were detected in samples separated under reducing conditions (Figure 3A, WB: anti-CoA, Lanes 4-6). The incubation of *h*NME1 with CoASSCoA induced the formation of NME1 dimers, which were detected on Coomassie-stained gel and anti-NME1 Western blot (Figure 3A, Lane 2), possibly mediated through thiol-disulfide exchange. The anti-CoA Western blot of NME1 treated with CoASSCoA shows CoAlation of both the monomeric and dimeric forms of NME1, but the former being the most prominent (Lane 2). The NME1 sample treated with H_2O_2, in the presence of CoA, shows immunoreactive bands which correspond to monomeric, dimeric and oligomeric forms of NME1, and are only observed under non-reduced conditions (Figure 3A, WB: anti-CoA – Lane 3). Notably, a faster migrating band of ~17 kDa was detected when *h*NME1 was incubated with CoA and H_2O_2 (Figure 3A, Lane 3). This faster migrating band which is also covalently modified by CoA could correspond to *h*NME1 with an intramolecular disulfide bond between Cys4 and Cys145, as previously observed (6).

The analysis of *h*NME1 CoAlation in bacteria was carried out in BL21 (DE3) cells transformed with the pET28a(+)-His-*h*NME1 plasmid. Oxidative stress was then induced by culturing IPTG-induced bacteria for 10 min with 2 mM diamide, or 10 mM H_2O_2. To stimulate hypochlorite (NaOCl) stress, the IPTG-induced bacterial culture was pelleted, resuspended in warm M9 minimal media (M9), and incubated for 5 min at 37°C, before the 10 min-treatment with 100 µM NaOCl. *h*NME1 was pulled-down from lysed cells using Ni-NTA beads and analysed together with total cell lysates by SDS–PAGE under non-reducing condition and Western blotting with anti-CoA antibody (Figure 3B and C). Anti-CoA Western blot analysis of total cell lysates shows that diamide induces strong protein CoAlation, while a weaker immunoreactive signal is observed in samples of H_2O_2- and NaOCl-treated cells (Figure 3B). Background immunoreactivity is detected in control samples and in cells cultured in minimal media for 10 min. Immunoblotting of pulled-down *h*NME1 with anti-CoA antibody showed several immunoreactive bands in cells exposed to oxidative stress, which correspond to monomeric, dimeric and oligomeric forms of NME1 (Figure 3C). In contrast to

546 controls, H_2O_2- and NaOCl-treated cells, the bulk of pulled-down *h*NME1 from cells exposed
547 to diamide stress migrates around 40 kDa. This immunoreactive band corresponds to a
548 major Ponceau-stained band on the Western blot membrane and represents the dimeric
549 form of *h*NME1. A weak anti-CoA immunoreactive signal, corresponding to monomeric and
550 dimeric forms of NME1 is also observed in nutrient-deprived cells. A background CoAlation
551 of *h*NME1 is detected in untreated control cells.
552
553 *3.4. NME1 is CoAlated in cellular response to oxidative and metabolic stresses in*
554 *HEK293/Pank1β cells*
555 Further analysis of NME1 CoAlation under oxidative or metabolic stress was carried
556 out in mammalian cells. Here, HEK293/Pank1β cells were transiently transfected with the
557 pTwist-CMV-His-*h*NME1 plasmid which drives the expression of *h*NME1. Transfected cells
558 were treated with or without 500 μM diamide or subjected to a H_2O_2 dose-course to induce
559 oxidative stress. Ni-NTA beads were used to pull down transiently overexpressed *h*NME1.
560 Pulled-down *h*NME1 was separated by SDS-PAGE gel under non-reducing conditions and
561 analysed by anti-CoA Western blotting (Figure 4A). Western blot with anti-CoA of pulled-
562 down samples showed readily detectable *h*NME1 CoAlation in cells treated with diamide
563 (Figure 4A) and a dose-dependent increase in H_2O_2-treated cells but not in the control
564 untreated cells (Figure 4B).
565 CoA functions as a key metabolic cofactor in all living cells, and therefore, we
566 examined *h*NME1 CoAlation in mammalian cells under metabolic stress (Figure 4C). In this
567 study, HEK293/Pank1β cells were transiently transfected with pTwist-CMV-His-*h*NME1
568 plasmid and subjected to glucose deprivation upon 20 h incubation in 5 mM glucose and
569 pyruvate-free DMEM media. Harvested cells were lysed and *h*NME1 was pulled-down using
570 Ni-NTA beads. Total cell lysates and pulled-down samples were separated by SDS-PAGE
571 gel under non-reducing conditions and immunoblotted with anti-CoA and anti-NME1
572 antibodies (Figure 4C and D). Three immunoreactive bands, corresponding to monomeric,
573 dimeric and much weaker, trimeric forms of CoAlated NME1 were detected in pulled-down
574 samples from cells under metabolic stress (Figure 4C). Extensive protein CoAlation is
575 observed in total protein lysates of cells exposed to metabolic stress in comparison to control
576 cells (Figure 4D). Altogether, our findings demonstrate that NME1 CoAlation is induced in
577 cellular response to oxidative stress and metabolic stress.

578 *3.5. Covalent and non-covalent binding of CoA to NME1 inhibits its NDPK activity.*
579 The development of the *in vitro* CoAlation assay allowed us to study the impact of
580 CoAlation on the activity of enzymes modified by covalent attachment of CoA, including
581 Aurora kinase A (AurKA), creatine kinase (CK), glyceraldehyde-3-phosphate dehydrogenase

582 (GAPDH) and peroxiredoxin 5 (PRDX5) (31, 35, 40). In most cases, the oxidative post-
583 translational modification (oxPTM) of enzymes by CoA resulted in significant inhibition of
584 their enzymatic activities. In this study, we explored the modulation of the NDPK activity of
585 NME1 by covalent and non-covalent binding of CoA.

586 To investigate the effect of CoAlation on NME1, the NDPK activity of reduced and *in*
587 *vitro* CoAlated NME1 was assayed spectrophotometrically. The assay involves three
588 reactions: i) within the first reaction, NME1 transfers the phosphate of ATP to dCDP via its
589 NDPK activity; ii) the ADP produced is then converted to ATP by pyruvate kinase. This
590 reaction converts ADP and PEP into ATP and pyruvate; iii) finally, pyruvate is converted to
591 lactate by PK in the presence of NADH. The latter reaction involves the consumption of
592 NADH, which can be spectrophotometrically monitored by following the decrease in $A_{340\ nm}$.
593 CoAlation of *h*NME1 significantly decreased the NME1 NDPK activity compared to the
594 reduced *h*NME1 sample (Figure 5A). These findings indicate that CoAlation negatively
595 regulates the NDPK activity of *h*NME1. To determine whether the activity of NME1 could be
596 restored following the removal of CoA, the CoAlated sample was incubated with DTT for 30
597 min at 25°C before measuring its NDPK activity. The inhibitory effect of CoAlation on NDPK
598 activity was nearly restored (to 84.8%) upon removal of CoA in the presence of DTT.

599 A C109A mutant of NME1 was recently shown to retain the NDPK activity under
600 oxidative stress (7). To demonstrate that Cys109 is the functional CoAlated residue which is
601 affecting the NDPK activity, we generated the NME1 C109A mutant and showed that its
602 NDPK activity was comparable to that of wild type (WT) *h*NME1. *In vitro* CoAlation of *h*NME1
603 C109A mutant had no effect on its NDPK activity (Figure 5A). These findings further confirm
604 the redox-sensitive nature of Cys109 in the regulation of the NDPK activity of NME1.

605 Having demonstrated that NME1 can bind CoA (Figure 1) and considering the
606 structural similarities between ATP and CoA, we hypothesised that CoA could bind the
607 nucleotide binding pocket and act as a competitive inhibitor. The NDPK activity of reduced
608 *h*NME1 WT and C109A mutant was assayed in the presence of increasing concentrations of
609 reduced CoA (0, 2, 4 mM) while the concentration of ATP used was kept constant at 2 mM.
610 Figure 5B demonstrates that CoA inhibits the NDPK activity of WT *h*NME1 (2 mM CoA- 43.3%
611 inhibition; 4mM CoA- 69.9% inhibition). To further examine whether Cys109 influences the
612 inhibition of NME1 by CoA, the same experiment was performed with the reduced form of
613 NME1 C109A mutant (Figure 5B). The results show that in the presence of CoA, the NDPK
614 activity of C109A mutant is also inhibited (2 mM CoA- 22.1% inhibition; 4 mM CoA- 58.1%).
615 Overall, we show that CoA decreases the NME1 NDPK activity in a CoAlation (disulfide
616 linkage to cysteine) independent manner. This suggests that CoA has potentially two binding
617 modes: i) covalently bound through Cys109 mixed disulfide bond (Figure 5A) and ii) non-
618 covalently bound to the nucleotide binding pocket (Figure 5B).

4. Discussion

In this study, we show for the first time that CoA binds covalently and non-covalently to the metastasis suppressor NME1, and as a consequence, negatively regulates its NDPK activity. Due to the structural homology provided by the ADP moiety of CoA, through non-covalent interactions, CoA could bind to the highly promiscuous nucleotide binding pocket of NME1, leading to the inhibition of its NDPK activity. When considering the mechanism and the relevance of CoA binding to NME1 within the context of cells, it is known that the concentration of ATP in the cytoplasm of mammalian cells ranges between 1-10 mM (47), which is approximately 100-fold higher than the cytoplasmic levels of CoA (0.014-0.14 mM) (21). As ATP is more abundant in exponentially growing cells, it would outcompete CoA for the nucleotide binding pocket of NME1 and would act as a phosphate donor for the generation of other pools of NTPs via the NDPK activity.

During oxidative or metabolic stress conditions, ATP levels could be eventually depleted (48, 49) and hence, this would increase the probability of CoA to bind to NME1. The crystal structure of NME1 in complex with ADP (50) shows that Cys109 is buried within the Kpn-loop, which in turn interacts with the nucleotide. We therefore propose that due to thermal fluctuation or Cys4/Cys145 oxidation (6), the Kpn-loop could undergo a conformational change, leading to the exposure and subsequent oxidation of Cys109. It is at this stage that the formation of a mixed disulfide bond with the thiol group of CoA can occur. Subsequently, the 3'-phospho-ADP moiety of CoA is accommodated within the nucleotide binding pocket of NME1 (Figure 5C). The structural rearrangements and functional implications of CoA binding to NME1 in physiological/pathophysiological conditions would be a topic of interest for future studies.

Besides its extensively studied role in metastasis suppression, several studies have converged towards evidence that NME1 and NME2 are implicated in the regulation of oxidative stress response in different types of organisms. In *Neurospora cressa* and *Arabidopsis thaliana* (*At*) cells harbouring a kinase-defective mutant of an NME1 orthologue, NDK-1 (NDK-1^{P72H}), show a decrease in catalase-1 and 3 (Cat-1 and Cat-3) levels, making them sensitive to oxidative, heat and light stress (51, 52). Furthermore, *At*-NDK-1 was found to directly interact with Cat-1. Cells overexpressing *At*-NDK-1 are shown to be more resilient against paraquat and H_2O_2 treatments (52). NDK-2 has also been shown to regulate the cellular redox state by modulating the level of ROS in *A. thaliana* cells. NDK-2 is directly involved in enhancing the phosphorylation and activity of H_2O_2-activated MAPKs, indicating a role of NDK-2 in MAPK signalling in plants (53). Moreover, in a mouse pro-B cell line (BAF3), NME1 and NME2 overexpression protect cells from H_2O_2-induced cell death (54).

NME1 deficiency was shown to sensitise primary human keratinocytes and mouse transformed hepatocytes to acute oxidative stress and impaired the activation of stress-activated protein kinases, JNK and MAPK, which are dependent on the NDPK activity of NME1 (55). Increased sensitivity to acute paraquat mediated-oxidative stress was also observed in the liver of NME1 deficient mice, which associated with decreased superoxide dismutase activity and the overexpression of several stress-response genes, including glutathione transferases and glutathione reductase (55). Interestingly, in human cervical cancer cell line HeLa, NME1 was shown to co-immunoprecipitate with p53. The overexpression of NME1 in these cells, upregulated the expression of p53 as well as a p53-regulated gene *GPX1*, which encodes for the antioxidant enzyme, glutathione peroxidase 1, leading to increased cellular viability and resistance to oxidative stress (56). These studies demonstrate that the involvement of NME1 and NME2 in the oxidative stress response is conserved across different species, where both enzymes interact directly with stress response proteins (e.g. catalase in plants and fungi) or indirectly as an upstream signal transducer of signalling pathways involved in stress response (e.g. MAPK pathways, JNK signalling and p53). From our findings that indicate NME1 and NME2 are major CoA-binding proteins in mammalian cells and tissues, we speculate that CoA could be involved in the redox regulation of NME1 and NME2 activities (dependent on ATP/ADP:CoA ratio and the oxidative state of the cell), mediating the downstream stress response signalling pathways.

While the importance of two-component histidine kinases in bacteria, fungi and plants has long been recognised, very little is known about mammalian histidine kinases and histidine phosphatases due to the acid-labile nature of phosphohistidines, which are not detectable with commonly practised experimental techniques (57, 58). NME1,2,4 and 7 have been shown to act as histidine kinases through autophosphorylation on their active site histidine, followed by the transfer of the phosphoryl group to histidine residues on target proteins. Some known histidine phosphorylation targets of NMEs include, potassium channel KCa3.1(59) and calcium channel TRPV5 (60) by NME2 and, aldolase C (61), ATP-citrate lyase (62), succinate thiokinase (succinyl-CoA synthetase) (63) by NME1. The latter two enzymes are involved in CoA metabolism, where (i) ATP-citrate lyase catalyses the conversion of citrate to acetyl-CoA and links carbohydrate metabolism to fatty acid biosynthesis; and (ii) succinate thiokinase catalyses the reversible reaction of succinyl-CoA to succinate. These may provide some insights into the relevance of CoA-binding to NME1 and its impact on the physiological/ pathophysiological functions of NME1.

5. Conclusion

The findings presented in this study reveal NME1 as a novel CoA-binding partner. We report two modes of NME 1 regulation by CoA: (i) through non-covalent interactions, capable of competing with ATP; and (ii) through covalent modification by forming mixed disulfide bonds with redox-sensitive cysteines. Our proposed model suggests that CoA binds to NME1 during cellular oxidative stress via a dual anchoring to Cys109 and then onto the nucleotide binding pocket of NME1, with its pantetheine thiol and ADP moiety, respectively (Figure 5C). This study opens a novel avenue towards the exploration of NME1 regulation under oxidative or metabolic stress by an essential metabolic cofactor CoA, which has been recently found to function as a major cellular antioxidant. NME1 is a moonlighting enzyme, which interacts with various binding partners (small and large GTPases, GDP-GTP exchange factor TIAM1, DNA repair and redox regulation transcriptional factor APAX1; pro-apoptotic protease granzyme A) to mediate important cellular processes including maintaining intracellular nucleotide homeostasis, endocytosis, intracellular trafficking, stress-response signalling, cell motility and tumour metastasis (2, 3). Uncovering the role of CoA in the regulation of the diverse NME1 functions could help us understand further the involvement of CoA in cellular redox signalling and possibly in tumour metastasis.

In addition to NME1, the MS-based analysis of CoAlated proteins in diamide-treated HEK293/Pank1β cells revealed over 20 CoA-modified kinases, that catalyse the transfer of phosphate groups from ATP to a diverse range of substrates. The list includes pyruvate kinase, mTOR kinase, creatine kinase, Aurora A kinase, pantothenate kinase, DNA-PK catalytic subunit and thymidylate kinase among others (Table S1). The mode of CoA binding and regulation of kinases with different substrate specificity in cellular response to oxidative and metabolic stress will be an interesting avenue for future studies.

We have recently reported a novel mode of redox-regulated inhibition of Aurora A kinase by CoA, which locks the kinase in an inactive state via a “dual anchor” mechanism involving selective binding of the ADP moiety of CoA to the ATP binding pocket and covalent modification of Cys290 in the activation loop by the thiol group of the pantetheine tail (40). In the large family of protein kinases, the cysteine residue in the activation loop is found in approximately 30% of kinases. They are predominantly surface-exposed, and therefore, may function as targets for redox modifications and signaling. Further bioinformatics analysis of CoAlation sites in protein kinases showed that cysteine CoAlation could also occur in other regulatory regions, which are distant from the ATP binding pocket and may involve a different mode of regulation. Indeed, we found a protein kinase which is allosterically activated by covalent CoA binding (unpublished data). Therefore, the redox-mediated regulation of kinases by CoA is an emerging and promising field of research.

Authorship contribution statement

724 The present study was conceived by I.G.; M.-A.T., B.Y.K.Y. and I.G. designed the
725 experiments; B.Y.K.Y., M.-A.T., S.D.H., R.L., P.A. and Y.T. performed the experiments; S.P.-
726 C. and M.S. performed the MS analysis; V.F. coordinated the development and production of
727 the anti-CoA monoclonal antibody; B.Y.K.Y., M.-A.T., S.D.H., R.L., R.A., S.O., J.G. and I.G.
728 analysed and discussed generated results; B.Y.K.Y., M.-A.T., S.D.H., R.L. and I.G. wrote the
729 manuscript with the assistance and approval of all authors. All authors have read and agreed
730 to the published version of the manuscript.

731 **Funding**

732 This work was supported by grants to I.G. (UCLB 13-014 and 11-018; Rosetrees Trust
733 CM239-F2; BBSRC BB/L010410/1 and BB/S009027/1).

734

735 References:

736 1. Boissan M, Dabernat S, Peuchant E, Schlattner U, Lascu I, Lacombe ML. The mammalian
737 Nm23/NDPK family: from metastasis control to cilia movement. Mol Cell Biochem. 2009;329(1-2):51-
738 62.
739 2. Boissan M, Schlattner U, Lacombe ML. The NDPK/NME superfamily: state of the art. Lab
740 Invest. 2018;98(2):164-74.
741 3. Matyasi B, Farkas Z, Kopper L, Sebestyen A, Boissan M, Mehta A, et al. The Function of
742 NM23-H1/NME1 and Its Homologs in Major Processes Linked to Metastasis. Pathol Oncol Res.
743 2020;26(1):49-61.
744 4. Lu Z, Hunter T. Metabolic Kinases Moonlighting as Protein Kinases. Trends Biochem Sci.
745 2018;43(4):301-10.
746 5. Mesnildrey S, Agou F, Karlsson A, Deville Bonne D, Véron M. Coupling between catalysis and
747 oligomeric structure in nucleoside diphosphate kinase. Journal of Biological Chemistry.
748 1998;273(8):4436-42.
749 6. Kim MS, Jeong J, Jeong J, Shin DH, Lee KJ. Structure of Nm23-H1 under oxidative conditions.
750 Acta Crystallogr D Biol Crystallogr. 2013;69(Pt 4):669-80.
751 7. Lee E, Jeong J, Kim SE, Song EJ, Kang SW, Lee KJ. Multiple functions of Nm23-H1 are
752 regulated by oxido-reduction system. PLoS One. 2009;4(11):e7949.
753 8. Lin KH, Wang WJ, Wu YH, Cheng SY. Activation of antimetastatic Nm23-H1 gene expression
754 by estrogen and its alpha-receptor. Endocrinology. 2002;143(2):467-75.
755 9. Wong KM, Song J, Saini V, Wong YH. Small Molecules as Drugs to Upregulate Metastasis
756 Suppressors in Cancer Cells. Curr Med Chem. 2019;26(32):5876-99.
757 10. Hartsough MT, Clare SE, Mair M, Elkahloun AG, Sgroi D, Osborne CK, et al. Elevation of
758 breast carcinoma Nm23-H1 metastasis suppressor gene expression and reduced motility by DNA
759 methylation inhibition. Cancer Research. 2001;61(5):2320-7.
760 11. Chen W, Xiong S, Li J, Li X, Liu Y, Zou C, et al. The Ubiquitin E3 Ligase SCF-FBXO24 Recognizes
761 Deacetylated Nucleoside Diphosphate Kinase A To Enhance Its Degradation. Molecular and Cellular
762 Biology. 2015;35(6):1001-13.
763 12. Fiore LS, Ganguly SS, Sledziona J, Cibull ML, Wang C, Richards DL, et al. C-Abl and Arg induce
764 cathepsin-mediated lysosomal degradation of the NM23-H1 metastasis suppressor in invasive cancer.
765 Oncogene. 2014;33(36):4508-20.
766 13. Khan I, Steeg PS. Metastasis suppressors: Functional pathways. Laboratory Investigation.
767 2018;98(2):198-210.
768 14. Leone A, Flatow U, King CR, Sandeen MA, Margulies IMK, Liotta LA, et al. Reduced tumor
769 incidence, metastatic potential, and cytokine responsiveness of nm3-transfected melanoma cells.
770 Cell. 1991;65(1):25-35.
771 15. Palmieri D, Horak CE, Lee J-H, Halverson DO, Steeg PS. Translational approaches using
772 metastasis suppressor genes. Journal of bioenergetics and biomembranes. 2006;38(3-4):151-61.
773 16. Boissan M, Wendum D, Arnaud-Dabernat S, Munier A, Debray M, Lascu I, et al. Increased
774 lung metastasis in transgenic NM23-null/SV40 mice with hepatocellular carcinoma. Journal of the
775 National Cancer Institute. 2005;97(11):836-45.
776 17. Boissan M, De Wever O, Lizarraga F, Wendum D, Poincloux R, Chignard N, et al. Implication
777 of metastasis suppressor NM23-H1 in maintaining adherens junctions and limiting the invasive
778 potential of human cancer cells. Cancer Research. 2010;70(19):7710-22.
779 18. Leonardi R, Zhang YM, Rock CO, Jackowski S. Coenzyme A: Back in action. Progress in Lipid
780 Research. 2005;44(2-3):125-53.
781 19. Theodoulou FL, Sibon OCM, Jackowski S, Gout I. Coenzyme A and its derivatives: Renaissance
782 of a textbook classic. Biochemical Society Transactions. 2014;42(4):1025-32.

20. Baković J, López Martínez D, Nikolaou S, Yu BYK, Tossounian M-A, Tsuchiya Y, et al. Regulation of the CoA Biosynthetic Complex Assembly in Mammalian Cells. International Journal of Molecular Sciences. 2021;22(3).
21. Czumaj A, Szrok-Jurga S, Hebanowska A, Turyn J, Swierczynski J, Sledzinski T, et al. The pathophysiological role of CoA. International Journal of Molecular Sciences. 2020;21(23):1-30.
22. Martinez DL, Tsuchiya Y, Gout I, Lopez Martinez D, Tsuchiya Y, Gout I. Coenzyme A biosynthetic machinery in mammalian cells. Biochemical Society Transactions. 2014;42(4):1112-7.
23. Yu Y, Moretti IF, Grzeschik NA, Sibon OCM, Schepers H. Coenzyme A levels influence protein acetylation, CoAlation and 4′ -phosphopantetheinylation: Expanding the impact of a metabolic nexus molecule. Biochimica et Biophysica Acta (BBA) - Molecular Cell Research. 2021;1868(4):118965-.
24. Brass EP, Tahiliani AG, Allen RH, Stabler SP. Coenzyme A metabolism in vitamin B-12-deficient rats. Journal of Nutrition. 1990;120(3):290-7.
25. Corkey BE, Hale DE, Glennon MC, Kelley RI, Coates PM, Kilpatrick L, et al. Relationship between unusual hepatic acyl coenzyme A profiles and the pathogenesis of Reye syndrome. The Journal of clinical investigation. 1988;82(3):782-8.
26. McAllister RA, Fixter LM, Campbell EHG. The effect of tumour growth on liver pantothenate, coa, and fatty acid synthetase activity in the mouse. British Journal of Cancer. 1988;57(1):83-6.
27. Reibel DK, Wyse BW, Berkick DA, Neely JR. Regulation of coenzyme A synthesis in heart muscle: Effects of diabetes and fasting. American Journal of Physiology - Heart and Circulatory Physiology. 1981;9(4):H606-H11.
28. Dusi S, Valletta L, Haack TB, Tsuchiya Y, Venco P, Pasqualato S, et al. Exome sequence reveals mutations in CoA synthase as a cause of neurodegeneration with brain iron accumulation. The American Journal of Human Genetics. 2014;94(1):11-22.
29. Iuso A, Wiersma M, Schüller H-J, Pode-Shakked B, Marek-Yagel D, Grigat M, et al. Mutations in PPCS, encoding phosphopantothenoylcysteine synthetase, cause autosomal-recessive dilated cardiomyopathy. The American Journal of Human Genetics. 2018;102(6):1018-30.
30. Zhou B, Westaway SK, Levinson B, Johnson MA, Gitschier J, Hayflick SJ. A novel pantothenate kinase gene (PANK2) is defective in Hallervorden-Spatz syndrome. Nature genetics. 2001;28(4):345-9.
31. Bakovic J, Yu BYK, Silva D, Chew SP, Kim S, Ahn SH, et al. A key metabolic integrator, coenzyme A, modulates the activity of peroxiredoxin 5 via covalent modification. Mol Cell Biochem. 2019;461(1-2):91-102.
32. Gout I. Coenzyme A, protein CoAlation and redox regulation in mammalian cells. Biochem Soc Trans. 2018;46(3):721-8.
33. Gout I. Coenzyme A: a protective thiol in bacterial antioxidant defence. Biochem Soc Trans. 2019;47(1):469-76.
34. Tossounian MA, Zhang B, Gout I. The Writers, Readers, and Erasers in Redox Regulation of GAPDH. Antioxidants (Basel). 2020;9(12).
35. Tsuchiya Y, Peak-Chew SY, Newell C, Miller-Aidoo S, Mangal S, Zhyvoloup A, et al. Protein CoAlation: a redox-regulated protein modification by coenzyme A in mammalian cells. Biochem J. 2017;474(14):2489-508.
36. Tsuchiya Y, Zhyvoloup A, Bakovic J, Thomas N, Yu BYK, Das S, et al. Protein CoAlation and antioxidant function of coenzyme A in prokaryotic cells. Biochem J. 2018;475(11):1909-37.
37. Zhyvoloup A, Yu BYK, Bakovic J, Davis-Lunn M, Tossounian MA, Thomas N, et al. Analysis of disulphide bond linkage between CoA and protein cysteine thiols during sporulation and in spores of Bacillus species. FEMS Microbiol Lett. 2020;367(23).
38. Malanchuk OM, Panasyuk GG, Serbin NM, Gout IT, Filonenko VV. Generation and characterization of monoclonal antibodies specific to Coenzyme A. Biopolymers and Cell. 2015;31(3):187-92.

832 39. Zhyvoloup A, Yu BYK, Baković J, Davis-Lunn M, Tossounian MA, Thomas N, et al. Analysis of
833 disulphide bond linkage between CoA and protein cysteine thiols during sporulation and in spores of
834 Bacillus species. FEMS Microbiology Letters. 2020;367(23).
835 40. Tsuchiya Y, Byrne DP, Burgess SG, Bormann J, Bakovic J, Huang Y, et al. Covalent Aurora A
836 regulation by the metabolic integrator coenzyme A. Redox Biol. 2020;28:101318.
837 41. Agarwal RP, Robison B, Parks RE, Jr. Nucleoside diphosphokinase from human erythrocytes.
838 Methods Enzymol. 1978;51:376-86.
839 42. Postel EH, Ferrone CA. Nucleoside diphosphate kinase enzyme activity of NM23-H2/PuF is
840 not required for its DNA binding and in vitro transcriptional functions. J Biol Chem.
841 1994;269(12):8627-30.
842 43. Cox J, Mann M. MaxQuant enables high peptide identification rates, individualized p.p.b.-
843 range mass accuracies and proteome-wide protein quantification. Nat Biotechnol. 2008;26(12):1367-
844 72.
845 44. Engel C, Wierenga R. The diverse world of coenzyme A binding proteins. Curr Opin Struct
846 Biol. 1996;6(6):790-7.
847 45. Lundgren DH, Hwang SI, Wu L, Han DK. Role of spectral counting in quantitative proteomics.
848 Expert Rev Proteomics. 2010;7(1):39-53.
849 46. Vieira PS, de Giuseppe PO, de Oliveira AHC, Murakami MT. The role of the C-terminus and
850 Kpn loop in the quaternary structure stability of nucleoside diphosphate kinase from Leishmania
851 parasites. J Struct Biol. 2015;192(3):336-41.
852 47. Zimmerman JJ, von Saint André-von Arnim A, McLaughlin J. Chapter 74 - Cellular Respiration.
853 In: Fuhrman BP, Zimmerman JJ, editors. Pediatric Critical Care (Fourth Edition). Saint Louis: Mosby;
854 2011. p. 1058-72.
855 48. Tiwari BS, Belenghi B, Levine A. Oxidative stress increased respiration and generation of
856 reactive oxygen species, resulting in ATP depletion, opening of mitochondrial permeability transition,
857 and programmed cell death. Plant Physiol. 2002;128(4):1271-81.
858 49. Zhang X, Wu XQ, Lu S, Guo YL, Ma X. Deficit of mitochondria-derived ATP during oxidative
859 stress impairs mouse MII oocyte spindles. Cell Res. 2006;16(10):841-50.
860 50. Giraud MF, Georgescauld F, Lascu I, Dautant A. Crystal structures of S120G mutant and wild
861 type of human nucleoside diphosphate kinase A in complex with ADP. J Bioenerg Biomembr.
862 2006;38(3-4):261-4.
863 51. Yoshida Y, Ogura Y, Hasunuma K. Interaction of nucleoside diphosphate kinase and catalases
864 for stress and light responses in Neurospora crassa. FEBS Lett. 2006;580(13):3282-6.
865 52. Fukamatsu Y, Yabe N, Hasunuma K. Arabidopsis NDK1 is a component of ROS signaling by
866 interacting with three catalases. Plant Cell Physiol. 2003;44(10):982-9.
867 53. Moon H, Lee B, Choi G, Shin D, Prasad DT, Lee O, et al. NDP kinase 2 interacts with two
868 oxidative stress-activated MAPKs to regulate cellular redox state and enhances multiple stress
869 tolerance in transgenic plants. Proc Natl Acad Sci U S A. 2003;100(1):358-63.
870 54. Arnaud-Dabernat S, Masse K, Smani M, Peuchant E, Landry M, Bourbon PM, et al. Nm23-
871 M2/NDP kinase B induces endogenous c-myc and nm23-M1/NDP kinase A overexpression in BAF3
872 cells. Both NDP kinases protect the cells from oxidative stress-induced death. Exp Cell Res.
873 2004;301(2):293-304.
874 55. Peuchant E, Bats ML, Moranvillier I, Lepoivre M, Guitton J, Wendum D, et al. Metastasis
875 suppressor NM23 limits oxidative stress in mammals by preventing activation of stress-activated
876 protein kinases/JNKs through its nucleoside diphosphate kinase activity. FASEB J. 2017;31(4):1531-
877 46.
878 56. An R, Chu YL, Tian C, Dai XX, Chen JH, Shi Q, et al. Over-expression of nm23-H1 in HeLa cells
879 provides cells with higher resistance to oxidative stress possibly due to raising intracellular p53 and
880 GPX1. Acta Pharmacol Sin. 2008;29(12):1451-8.
881 57. Besant PG, Attwood PV. Mammalian histidine kinases. Biochim Biophys Acta. 2005;1754(1-
882 2):281-90.

883 58. Fuhs SR, Hunter T. pHisphorylation: the emergence of histidine phosphorylation as a
884 reversible regulatory modification. Curr Opin Cell Biol. 2017;45:8-16.
885 59. Srivastava S, Li Z, Ko K, Choudhury P, Albaqumi M, Johnson AK, et al. Histidine
886 phosphorylation of the potassium channel KCa3.1 by nucleoside diphosphate kinase B is required for
887 activation of KCa3.1 and CD4 T cells. Mol Cell. 2006;24(5):665-75.
888 60. Cai X, Srivastava S, Surindran S, Li Z, Skolnik EY. Regulation of the epithelial Ca(2)(+) channel
889 TRPV5 by reversible histidine phosphorylation mediated by NDPK-B and PHPT1. Mol Biol Cell.
890 2014;25(8):1244-50.
891 61. Wagner PD, Vu ND. Histidine to aspartate phosphotransferase activity of nm23 proteins:
892 phosphorylation of aldolase C on Asp-319. Biochem J. 2000;346 Pt 3:623-30.
893 62. Wagner PD, Vu ND. Phosphorylation of ATP-citrate lyase by nucleoside diphosphate kinase. J
894 Biol Chem. 1995;270(37):21758-64.
895 63. Wagner PD, Steeg PS, Vu ND. Two-component kinase-like activity of nm23 correlates with its
896 motility-suppressing activity. Proc Natl Acad Sci U S A. 1997;94(17):9000-5.

897

Table 1. NME1-4 are identified by LC-MS/MS analysis as CoA-binding proteins. The normalised total spectrum count refers to the total spectra established for a single protein.

HEK293/Pank1β cells				
Protein	**Accession number**	**Molecular weight (kDa)**	**Subcellular localisation**	**Normalised Total spectral count**
NME1 (NDPKA)	NDKA_HUMAN (P15531)	17	Cytoplasm Plasma membrane	411
NME2 (NDPKB)	NDKB_HUMAN (P22392)	17	Cytoplasm Midbody ring	395
NME3 (NDPKC)	NDK3_HUMAN (Q13232)	19	Nucleoplasm Cytoplasm	13
NME4 (NDPKD)	NDKM_HUMAN (O00746)	21	Mitochondria	15
Rat heart				
Protein	**Accession number**	**Molecular weight (kDa)**	**Subcellular localisation**	**Total spectral count**
NME1 (NDPKA)	NDKA_RAT (Q05982)	17	Cytoplasm Plasma membrane	623

NME2 (NDPKB)	NDKB_RAT (P19804)	17	Cytoplasm Midbody ring	855
NME3 (NDPKC)	Q99NI1_RAT (Q99NI1)	19	Nucleoplasm Cytoplasm	17
NME4 (NDPKD)	D3ZMT9_RAT (D3ZMT9)	21	Mitochondria	10

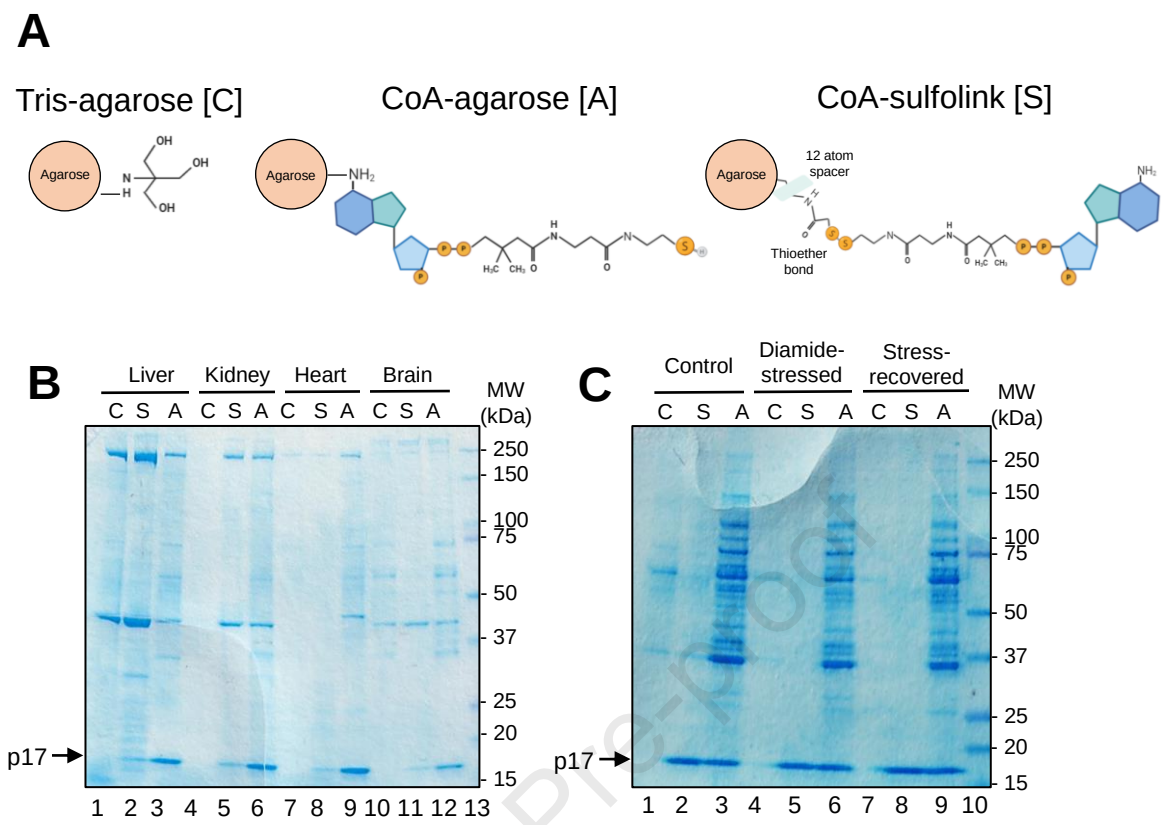

Figure 1. SDS-PAGE analysis of CoA-binding proteins from rat tissue and HEK293/Pank1β cell lysates. (A) Schematic diagrams of affinity matrices used in this study: Tris-agarose control beads [C], CoA-agarose [A] and CoA-sulfolink [S]. **(B)** Lysates of rat liver, kidney, brain and heart tissues were incubated with affinity matrices, bound proteins separated by SDS-PAGE and visualised by Coomassie staining; **(C)** Lysates of untreated, diamide-treated (500 µM) or stress-recovered HEK293/Pank1β cells were probed with affinity matrices and the bound proteins were separated by SDS-PAGE, and visualised by Coomassie staining. The arrows indicate a ~17 kDa protein which binds specifically to both CoA-affinity matrices, when compared to control beads. The figures shown are indicative of at least three independent repeats.

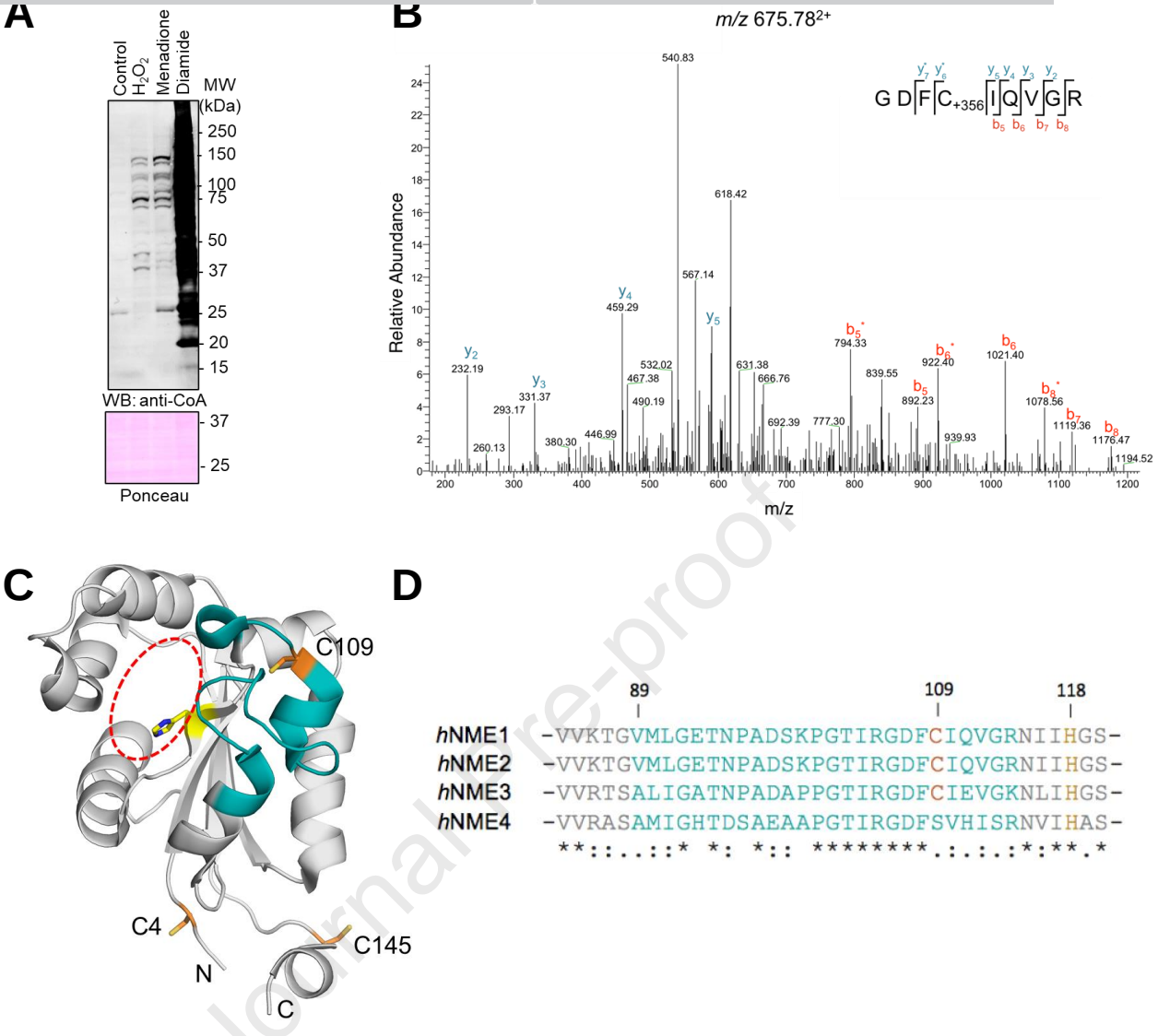

Figure 2. *h*NME1 is CoAlated at its redox-sensitive Cys109 in diamide-treated HEK293/Pank1β cells. (A) Anti-CoA Western blot reveals extensive modification of cellular proteins by CoA in HEK293/Pank1β cells treated with 500 μM diamide for 30 min, when compared to untreated cells; **(B)** The LC-MS/MS spectrum of the peptide (GDFC^{109}IQVGR) corresponding to NME1, containing CoA-modified cysteine (C+356) at residue 109 was obtained as described in Methods from HEK293/Pank1β cells treated with diamide. Fragment ions are coloured cyan and red for y- and b-ions, respectively. The asterisks (*) denote the loss of phosphoric acid (-98 Da) from the precursor and/ or product ions that contained the CoA-modified cysteine residue. **(C)** The X-ray crystal structure of *h*NME1 (PDB: 3L7U) is shown. The nucleotide binding pocket is indicated by a red ellipse, catalytic histidine residue (His118) in yellow and cysteine residues (Cys4, Cys109 and Cys145) in orange. The Kpn-loop (residues 89-114) is coloured in cyan. **(D)** The multiple sequence alignment of NME1-4 from residues 89 to 120 is shown. The redox-sensitive cysteine 109 is shown in orange, and conserved catalytic histidine 118 in yellow. The Kpn-loop (residues 89-114) of NME is shown in cyan. The residue numbering is based on the amino acid sequence of NME1.

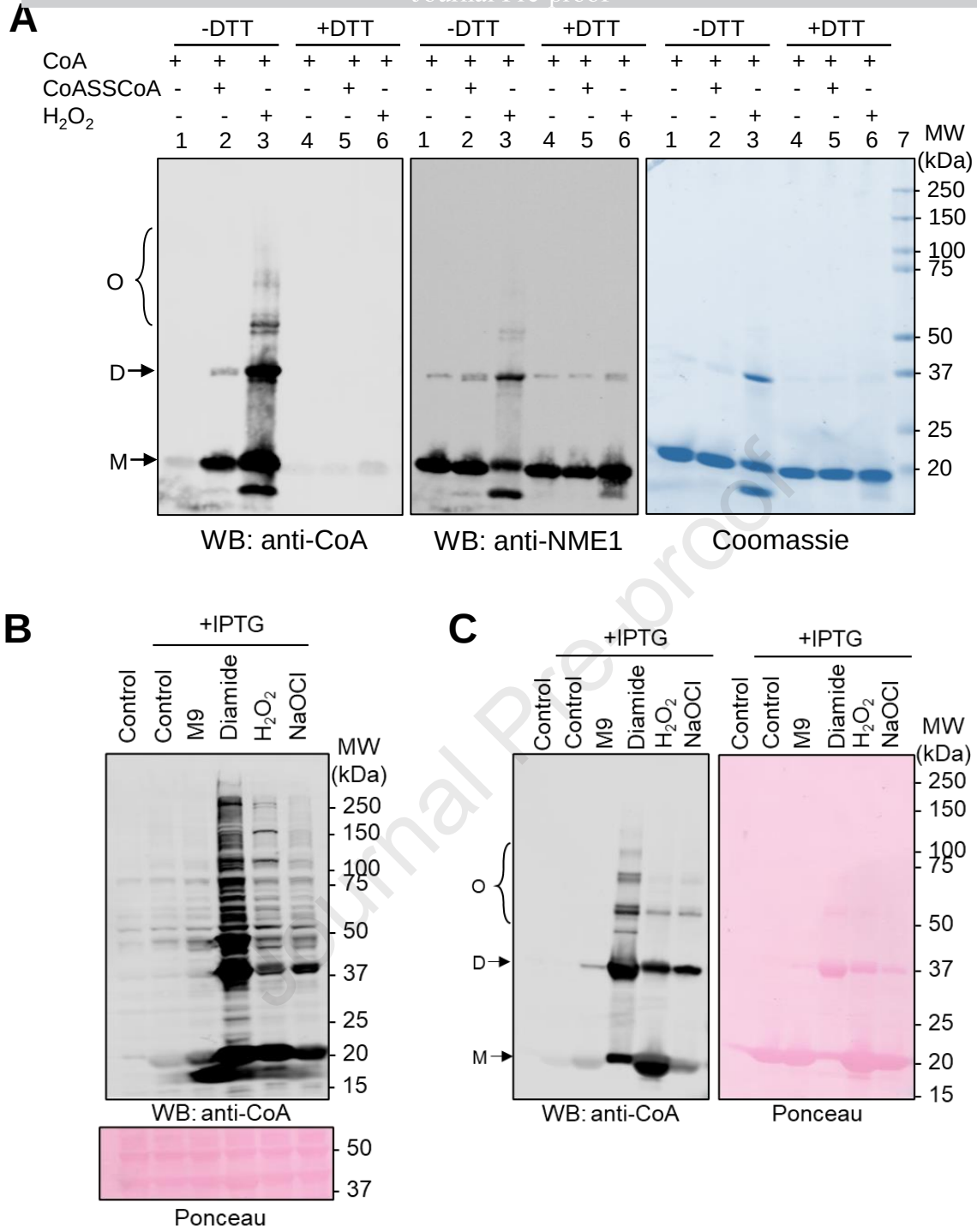

Figure 3. NME1 is CoAlated *in vitro* and in cellular response to oxidative and metabolic stress. (**A)** *In vitro* CoAlation of recombinant *h*NME1. *In vitro* CoAlation of 100 µM *h*NME1 was carried out in the presence of 400 µM CoASH; 400 µM CoASSCoA; or 700 µM CoASH and 2 mM H_2O_2. After buffer exchange, approximately 2 µg recombinant protein from each reaction was separated on SDS-PAGE gel under reducing (with DTT) or non-reducing conditions (without DTT). Gels were immunoblotted with anti-CoA or anti-NME1 antibodies or stained with Coomassie Blue. **(B, C)** CoAlation of *h*NME1 overexpressed in *E. coli* is strongly induced by oxidizing agents, but weakly under glucose deprivation. The expression of *h*NME1 in *E. coli* transformed with pET28a(+)-*h*NME1 plasmid was induced with 0.5 mM IPTG for 18 h at 25°C. Then, bacterial cultures were treated with 2 mM diamide, 10 mM H_2O_2 or 100 µM NaOCl (in M9 media) for 10 min, or incubated in M9 medium for 10 min. Total bacterial lysates **(B)** and Ni-NTA Sepharose pulled-down samples **(C)** were separated by SDS-PAGE gel under non-reducing condition and immunoblotted with anti-CoA antibody. Monomers (M), dimers (D) or oligomers (O) of NME1 have been indicated. The Ponceau-stained membranes show the loading control. The figures shown are indicative of three independent repeats.

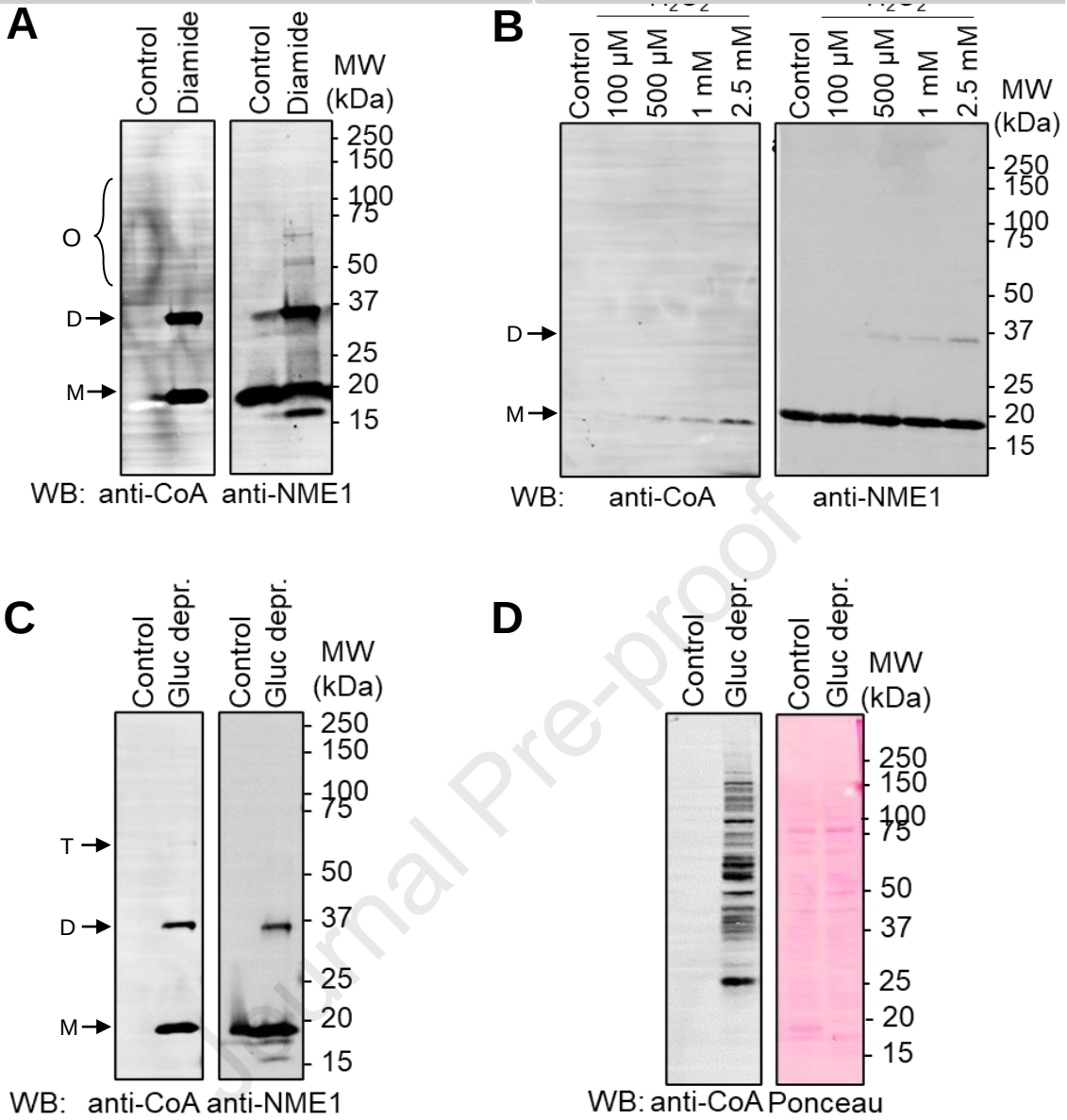

Figure 4. NME1 CoAlation in mammalian cells is induced by oxidising agents and glucose deprivation. (A,B) Anti-CoA and anti-NME1 Western blot analyses of affinity purified transiently overexpressed *h*NME1 from HEK293/Pank1β cells treated for 30 min with (**A**) 500 µM diamide, or **(B)** a dose-course of H_2O_2. **(C)** Anti-CoA and anti-NME1 Western blot analyses of affinity purified transiently overexpressed *h*NME1 from HEK293/Pank1β cells subjected to 20 h-glucose deprivation (Gluc depr.). **(D)** Anti-CoA and anti-NME1 Western blot analyses of total protein CoAlation in HEK293/Pank1β cells glucose deprived for 20 h. Ponceau stain shows equal loading of samples. Monomers (M), dimers (D), trimers (T) or oligomers (O) of NME1 have been indicated. All figures shown are representative of at least three independent repeats. The anti-NME1 Western blots represent the respective amounts of NME1 purified from each sample for analysis **(A-C)**.

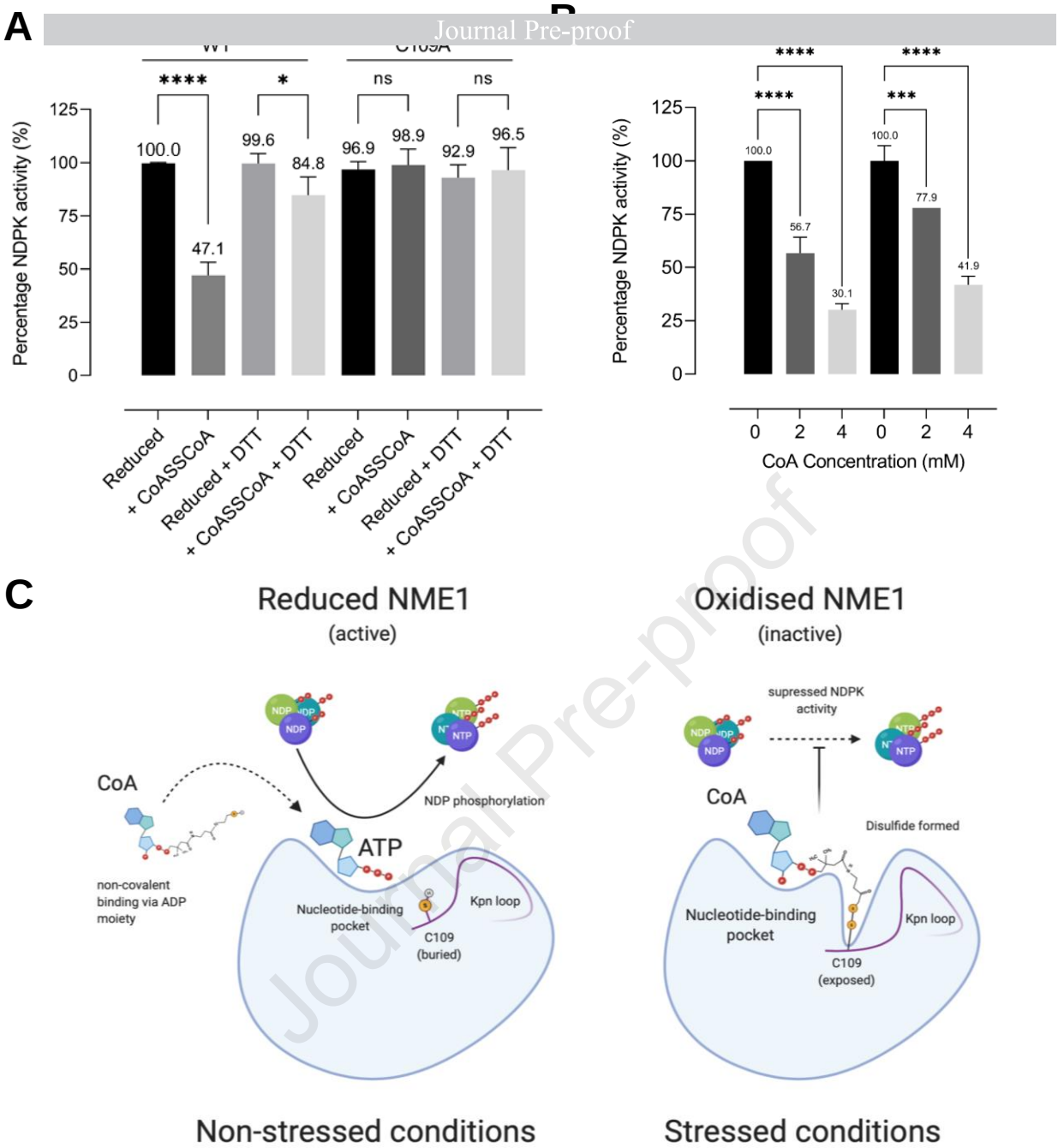

Figure 5. CoAlation of *h*NME1 inhibits its NDPK activity. (A) Upon incubation with CoASSCoA, the NDPK activity of *h*NME1 WT is reduced by ~53%. In the presence of DTT, which reduces the mixed disulfide bond between CoA and *h*NME1, the NDPK activity is restored up to 84.8%. CoAlation of *h*NME1 C109A mutant shows no reduction in NDPK activity. In the absence of Cys109, CoAlation does not occur close to the active site and therefore, *h*NME1 maintains its NDPK activity. Data represent mean ± SEM from n = 2 or 3 experiments. p values were calculated using Šidák multiple comparison, ordinary one-way ANOVA test (**** $p < 0.0001$, * $p < 0.05$, ns= not significant). **(B)** NDPK activity of *h*NME1 WT and C109A mutant was measured in the presence of increasing concentrations of reduced CoA (0, 2 and 4 mM). Results show that non-covalently bound CoA to both *h*NME1 WT and C109A mutant competitively inhibits their NDPK activity. The data are presented as a mean ± S.D. of at least three independent experiments. Data represent mean ± SEM from n = 2 or 3 experiments. p values were calculated using Šidák multiple comparison, ordinary one-way ANOVA test (**** $p < 0.0001$, *** $p < 0.0006$). **(C)** Predictive model of CoA binding to NME1 under non-stressed and stressed cellular conditions. During non-stressed conditions, ATP binds to the active site of NME1 in order to initiate its NDPK activity. However, under cellular stress conditions, CoA may potentially bind non-covalently with its ADP moiety to the nucleotide-binding pocket of NME1; in this way, CoA may compete with ATP and other NTPs for the active site and possibly act as a competitive inhibitor for its NDPK activity. During oxidizing conditions, CoA can also form a mixed disulfide bond with Cys109. This is followed by the accommodation of the 3'-phospho-ADP moiety of CoA within the nucleotide binding pocket of NME1. Covalent anchoring of CoA onto NME1 would force NME1 into an inactive state.

Highlights

- NME1 is a major CoA-binding protein
- CoA can bind NME1 through covalent and non-covalent interactions
- NME1 CoAlation is induced by oxidative and metabolic stress in mammalian cells
- CoA inhibits the NDPK activity of NME1 *in vitro*

Re: Manuscript number: REDOX-D-21-00182

" Regulation of metastasis suppressor NME1 by a key metabolic cofactor coenzyme A "

All authors of this manuscript declare no conflict of interest.

Corresponding author

Dr. Ivan Gout